THESIS

A DYNAMIC ENGINEERING MODEL OF ALGAL CULTIVATION SYSTEMS

Submitted by

Samuel Lighthall Compton

Department of Mechanical Engineering

In partial fulfillment of the requirements

For the Degree of Master of Science

Colorado State University

Fort Collins Colorado

Fall 2017

Master's Committee:

Advisor: Jason C. Quinn

Anthony Marchese
Graham Peers

ABSTRACT

A DYNAMIC ENGINEERING MODEL OF ALGAL CULTIVATION SYSTEMS

Proper assessment of the sustainability of algal products is constrained by the onerous process of pilot-scale experimental study. This study developed a bulk growth model that utilizes strain characterization, geospatial data, and cultivation platform geometry to predict productivity across different outdoor systems. The model interprets a minimum of measureable algal strain characteristics along with characteristics of the growth architecture to calculate a time-resolved algal concentration. Validation of the model illustrates an average accuracy of 7.33%+/- 5.65% for photobioreactors (PBR) and 6.7%+/- 5.33% for an open raceway pond (ORP) across five total species: *Chlorella vulgaris, Desmodesmus intermedius, Galdieria sulphuraria, Galdieria sulphuraria Soos,* and *Nannochloropsis oceanica.* The validated model assesses productivity at several locations in the United States with *Chlorella vulgaris,* grown in open raceway ponds and *Galdieria sulphuraria* grown in vertical flat panel photobioreactors. The model investigates seasonal variability through geospatially and temporally resolved extrapolation.

ACKNOWLEDGEMENTS

I would like to acknowledge financial support from the United States Department of Energy (DE-EE0007562). Myself, and all collaborating authors, also thank Danna Quinn for support in editing the manuscript of the journal submission core to the content of this thesis. Mark Seger, Thinesh Selvaratnam, and Nicholas Csakan from the ASU School of Sustainable Engineering and the Build Environment are also acknowledged for their experimental support. Finally, recognition is due to OpenEI.org and the Algae Testbed Public Private Partnership for support in supplying and web-hosting validation data.

TABLE OF CONTENTS

INTRODUCTION[1]

Algal biomass cultivation is an attractive means of providing an environmental service through water treatment and carbon dioxide utilization while producing a valuable biomass product. Via fixation of atmospheric carbon dioxide during photosynthetic growth, algae can convert atmospheric carbon to a complex, organic, chemical matrix that may be exploited for a variety of bio-based downstream products. Several techno-economic and lifecycle assessments, applied to algal biofuels processes, have shown a range of environmental benefits and economic fuel selling prices [1,2]. However, research has also demonstrated that sustainability assessments of algae biomass processes often retain dramatic sensitivity to the values of algal biomass productivity in the growth architecture of interest [2–4]. Recent studies have identified the importance of temporally and geographically resolved growth modeling for accurate assessment of the process [3,4]. Modeling of the algal biomass growth process, at high fidelity, can provide a better understanding of realistic expectations of algal biomass growth systems. Moreover, an accurate algal growth model can serve as a platform for resource assessment and system optimization.

Some preexisting studies, though logically sound, lack experimental validation[5–7]. In other cases, the time and physical scale of the model and its experimental counterpart are ill suited to predictions of algal productivity on a pilot or commercial scale [8,9]. Other approaches, often employing an otherwise sound approach, validate their modelling method to a single

[1] The content of this manuscript is from a 2017 submission to Environmental Science and Technology by Samuel Compton, Peter J. Lammers, and Jason C. Quinn titled “Bulk growth model of algal productivity in various outdoor cultivation platforms” currently in review. Reproduced in part with permission from Environmental Science and Technology, submitted for publication. Unpublished work copyright 2017 American Chemical Society.

growth system architecture or strain of algae[10–12]. Other growth models have made simplistic assumptions such as a fixed photosynthetic conversion efficiency, conversion efficiencies irrespective of growth architecture geometry, or an absence of coupling between dynamic culture conditions and productivity[13,14].

Based on the current state of the field, there exists a need to develop a dynamic bulk growth model that requires minimal strain characterization data and has the ability to predict productivity across a diverse set of growth architectures. The modeling effort in this study develops a thermal model of an open raceway pond (ORP) and a vertical flat panel photobioreactor (VFP PBR) and couples it with a bulk algal growth model to predict algal productivity. Data inputs are comprised of an algal strain's temperature responsiveness, response to varying light-intensity, and typical optical density regression. Other primary input parameters to the model include growth architecture characteristic length and meteorological data. The model was validated across multiple species cultivated outdoors in ORPs or PBRs utilizing two different data sources. First, publically available data from the Algae Testbed Public-Private-Partnership (ATP^3) test bed trials for *Chlorella vulgaris* (LRB-AZ-1201), *Nannochloropsis oceanica* (KA32), *and Desmodesmus intermedius* (C046), at two locations: Mesa, AZ (Arizona Center for Algal Technology and Innovation (AzCATI) and Atlanta, GA (Georgia Institute of Technology) [15,16]. The second data set was for two strains of red algae: *Galdieria sulphuraria* CCMEE 5587.1 (hereafter *G. sulphuraria*) and *G. sulphuraria Soos* [17–19].

Sensitivity analysis highlights the high impact model input variables, notably the geometric characteristics of the growth architecture and ambient conditions affecting the culture conditions. The model couples with meteorological data to understand productivity potential in various geographical locations including seasonal variability. The modeling approach developed in this

study is a method for comparing algal biomass cultivation strategies across regions, growth architectures, and strains that do not require prohibitive experimental data inputs.

MATERIALS AND METHODS

The modeling approach developed in this study couples a thermal model that calculates culture temperature based on weather conditions to a biological model that calculates time-resolved growth rates based on culture temperature and light conditions. Both the thermal and biological models were validated independently against experimental trials with concurrent weather data measurement. When coupled, the thermal model and biological growth model rely on inputs of growth architecture characteristics, geographic and weather data, and a basic characterization of the algae strain of interest, to provide a time resolved understanding of algal culture conditions within a growth system. The finished model provides a dynamic value of algal concentration over time.

Biological Model

Growth rate and time-integration

The growth model is based on an incident light correlated carbon fixation rate that is impacted by multiple efficiency factors. This study understands algal concentration according to the following governing linear, ordinary, differential equation:

$$\frac{dC_x}{dt} = \frac{\varphi_L \cdot \varphi_T \cdot \varphi_C \cdot P \cdot \emptyset_{photon}}{V} - D/V \qquad [1]$$

With C_x being the concentration of biomass in g m^{-3}, V being volume in m^3, D being the decay rate in g s^{-1}, P being the rate of photosynthetic spectrum photon incidence in µE/m^2*s, and φ_L, φ_T, φ_C, are dimensionless efficiency factors depending on incident light intensity, temperature, and concentration respectively. Each of the values of V, φ_L, φ_T, φ_C, P, and D are calculated at every discrete time step. Equation 1 is integrated numerically in time via an explicit, first-order,

time-marching method [20]. A time step size of 30 minutes for VFP PBR models and 1 hour for ORP models was utilized for the results presented in this study. Further reduction of time-step size below 30 minutes requires extensive conditioning of input data and presents an increasing computational burden with reduction below 1 hour for ORP models showing minimal improvement in results. Decreasing the time-step size showed minimal impact on model accuracy during validation efforts. Each of the variables in equation 1 are further defined including the foundational assumptions below.

The model of algal growth utilized in this study begins with a calculation of the maximum rate of biomass carbon accumulation based on the incident light intensity at the culture boundaries, measured in micro-moles of photosynthetic active radiation (PAR). The base, un-adjusted ratio of 12 photons to each carbon fixed is based on a stoichiometric understanding of the global photosynthesis cycle based on work by Wilhelm and Jakob[21]. Under the assumption that the algal biomass is approximately 50% carbon, based on Quinn et. al.[12], the maximum rate accumulation of dry algal biomass in the culture can then be calculated. The arithmetic supporting this relationship is available in the Appendix. However, as the study by Wilhelm and Jakob[21] shows, this idealized rate of mass accumulation would provide an inaccurate calculation of growth rate overtime as the real world introduces inefficiencies. Several modifiers adjust the idealized rate and account for real sub-optimal culture conditions. Calculations of the biomass growth rate assume that light is the primary limiting input to metabolic reactions, similar to the model developed by Bechet et al.[10].

Temperature Efficiency

To account for inefficiencies due to non-optimal culture temperature for the strain in question, a scaling factor is applied based on the method developed by Alexandrov and Yamagata[22].

$$\varphi_T = \frac{2 \cdot T}{(1+F(T)^2)} \qquad [2]$$

$$F(T) = \exp\left(\frac{Ea}{R \cdot T_{opt}} - \frac{Ea}{R \cdot T}\right) \qquad [3]$$

T, in these equations is temperature, in K, Ea is the activation energy for photosynthesis in J kg^{-1}, R is the ideal gas constant, and T_{opt} is the optimal temperature for algal growth for each strain. This efficiency factor, φ_T is a dimensionless value between 0 and 1. It has a value of unity at the optimal temperature and a sub-unity value at any other temperature.

Photolimitation and Photoinhibition

Existing research has shown that above and below a certain optimal irradiance point, the rate of algal photosynthesis diminishes [23,24]. Accordingly, the rate of biomass accumulation calculated in this model is scaled for that effect. For values under the optimal irradiance point, the model considers the photosynthetic state of the algae to be photo-limited. However, since the rate of biomass accumulation is directly proportional to the incident light intensity, the biomass accumulation rate is allowed to vary linearly, unadjusted up to the optimal light intensity. Above the optimal light intensity, the biomass accumulation rate is scaled by an exponentially decaying modifier whose values occupy the range between 1 and the minimum fraction of peak photosynthetic rate observed from experimental characterization of the strain in consideration.

$$\varphi_L = 1 \qquad \text{for } I < I_{opt} \qquad [4]$$

$$\varphi_L = \exp(-a \cdot (I - I_{opt})) \qquad \text{for } I_{opt} \leq I \leq I(\varphi_{L\,Min}) \qquad [5]$$

$$\varphi_L = \varphi_{L\,Min} \qquad \text{for } I > I(\varphi_{L\,Min}) \qquad [6]$$

Where φ_L is the light-intensity related efficiency, a is a dimensionless curvature coefficient, and $\varphi_{L\,Min}$ is the minimum light-intensity related efficiency. I is equal to the incident light, I_0, scaled for biomass concentration effects by φ_C.

Culture Opacity Effects

An observed effect of algal biomass in suspension is the diminished transparency of the culture from that of clear water [5,25–27]. To account for the effect of suspended algal solids, without spatial discretization of the growth architecture such as that shown in work by Yuan et al.[28], a volume-integral-average approach is applied to the Beer-Lambert Law. This approach relies on the assumptions that the culture is well-mixed; that the concentration of algal biomass is uniform throughout the growth architecture unit. A concentration efficiency factor, is calculated as follows and is based on the method shown in Quinn et al.[12]:

$$\varphi_C = \frac{\int_0^d \exp(-\alpha * Cx * z)dz}{\iiint dZdXdY} \qquad [7]$$

Where I_0 is the surface incident light intensity in W m^{-2}, α is the absorption coefficient, and z is an independent coordinate. This equation is applied to compute a volume-integral average for a characteristic length, d, dependent on geometry. This factor, φ_C is applied to the value of irradiance used to calculate the incident light efficiency, φ_L.

Respiration Decay

Respiratory losses in algal cultures are an imperative aspect of realistic growth models and represent a complex aspect of algae metabolism [12,23]. This study assumed that respiratory

biomass losses occur constantly in the form of photorespiration and mitochondrial respiration. Moreover, this model assumes that any metabolic scaling factors (φ_L, φ_T) that are applied to the positive growth rate are simultaneously applied to the respiratory biomass loss rate. At each point in time, the biomass loss rate is calculated based on the amount of algal biomass in the system coupled to the same temperature and light intensity efficiency factors applied to the positive growth rate. It is assumed that the opacity of the culture does not affect the negative metabolic rate of the culture; therefore, φ_c is not applied to the respiratory consumption of algal biomass. Shown below is an equation for this decay rate, D:

$$D = \varphi_L \cdot \varphi_T \cdot \emptyset_{respiration} \qquad [8]$$

with units of grams per second per unit algal biomass. Values and the method for determining $\emptyset_{respiration}$ are shown in the Appendix.

Thermal Model

Rigorous studies have shown dependence between temperature conditions within an algal culture and algal productivity [22–24,29,30]. The model presented in this study calculates a time-varying culture temperature based on changing weather conditions in a manner similar to preceding studies [5,7,31,32]. Unlike Endres et al.[6] and Slegers et al.[7], the thermal model developed in this study was validated against experimental temperature data with simultaneously observed weather conditions prior to developing any growth productivity results. This study uses the calculated temperature as a foundational input in the biological growth model. Moreover, the dynamic coupling between culture conditions and these inputs was considered vital to improving the fidelity of work compared to studies with static assumptions regarding this interplay [13,14].

A thermal model was coupled to the model of algal growth to maintain appropriate fidelity towards the critical variable of culture temperature during model extrapolation. Individual modes of heat transfer vary between the thermal model of an open raceway pond versus a vertical flat panel photobioreactor. However, in each case a transient energy balance equated to the rate of energy change of the entire unit is calculated and then integrated numerically in time. Weather data, collected at the experiment site in 15 minute intervals, was provided to the thermal model and temperatures were compared at each time interval. The thermal model, for both VFP PBR and ORP, was validated against experimental temperature data.

Vertical Flat Panel PBR Thermal Model

The thermal model of a VFP PBR employed in this study builds on the work by Endres et al. and Slegers et al.[6,7] with adjustments made based on feedback from experimental validation. In this model, heat fluxes are calculated based on weather conditions. The heat fluxes provide the basis for an energy balance as shown below [33].

$$\rho C_p V \frac{dT}{dt} = \sum Q_n \qquad [9]$$

Where ρ is the culture density, C_p is the culture specific heat in J kg^{-1} K^{-1}, V is volume, T is temperature, t is the independent time coordinate, and $\sum Q_n$ is the sum of all relevant heat fluxes. In the case of the VFP PBR, the fluxes considered in the $\sum Q_n$ term are convection with ambient air, direct solar irradiance, diffuse solar irradiance, distant atmospheric irradiance, ground reflection, irradiance from the ground, reflection between adjacent panels, radiation from adjacent panels, panel re-radiation, and evaporative cooling from sparging or evaporation to ambient air. Together, the right hand side of this equation is numerically integrated via a 4th

order Runge-Kutta time-marching method [20]. A summary of the flux equations applied in this model are available in the Appendix. Algorithms for determining the shaded portion and extent of radiation from reflection, as well as a summary of the flux equations in this model, are in the Appendix, and are an adaptation of existing methods published in the literature[6,7].

Open raceway pond thermal model

The thermal modeling approach in the model of an ORP follows a similar approach to that of the VFP and builds upon the work developed by Bechet et al.[34]. However, there are differences regarding the treatment of radiative fluxes between the VFP and ORP. Moreover, ground radiation and reflection are not considered in the ORP thermal model since the interfaces of the ORP control volume exposed to these fluxes are considered to be opaque. Values for global horizontal irradiance (GHI) are used to calculate the heat flux due to both direct and diffuse radiation, rather than meteorological measurements of diffuse horizontal irradiance (DHI) and direct normal irradiance (DNI), which are used in the thermal model of the VFP PBR. The usage of GHI for calculating heat flux due to solar irradiance provides a means of simplifying the model and enables coupling to the ATP^3 dataset, wherein DNI and DHI were not measured. Analogous to the VFP PBR thermal modelling approach is the development of an energy balance at each discrete time step and time integration therein via Runge-Kutta 4th order numerical integration [20].

Strain Characterization Requirements

The model structure used in this study was developed with a minimum of experimental strain characteristic metrics in mind. However, at some point the species specific dependence of algal response to culture conditions cannot be ignored. The metrics selected seek to succinctly capture the required variation in productivity response through readily measured quantities.

The characterization of algal species can be an experimentally intensive process. The objective of this study is to perform modeling based on minimal experimentally derived inputs. Since the temperature efficiency is assumed to match the shape developed in work by Alexandrov and Yamagata[22] only the optimum temperature needs to be identified, therefore simplifying the development of this data input. Similarly, a growth rate response varying solely with incident irradiance measured in μE m^{-2}, or unit readily converted to μE m^{-2}, is required. In both the instances of temperature efficiency curve development and photo-inhibition related efficiency curve development, the optimal point is of primary interest. In the case of photo-inhibition related efficiency, the curvature term a in equation 7 is informed by the progression of biomass productivity beyond the optimal. Since the photolimitation efficiency is a dimensionless value scaling between 0 and unity, the ratio of peak response to diminished response with varying incident light intensity will inform the curvature term, a. The optical density coefficient is developed from a linear curve-fit to optical density with varying algal concentration. The peak respiration rates used in this study were estimated by configuring all other aspects of the model, including the other strain characteristic inputs, and then seeking the respiration rate input that minimized error between model predicted final algal concentration and a single experimental trial final algal concentration. Reuse of this figure to the other biomass concentration values in a validation set suggests that this is a robust method. The values used for each strain characteristic input for the case studies and validation effort undertaken in this study are shown in Table S1.

Biological and Thermal Modeling Validation

Temperature and algal biomass productivity data used in the validation portion of this study came from two sources, trials performed at the Arizona Center for Algae Technology and

Innovation (AzCATI) and the ATP^3 testbed trials performed at AzCATI and the Georgia Institute of Technology [16]. The trials of *G. sulphuraria* 5587.1 were performed at AzCATI in VFP PBRs during the summer of 2016 with concurrent weather data collection. The ATP^3 testbed trials provided data for validation of the model developed in this study applied to *C. vulgaris, Desmodesmus intermedius,* and *Nannocholoropsis oceanica* cultivated in ORPs [16]. Cultures in this study were cultivated in approximately 1000 L open raceway ponds. *N. oceanica* trials were performed from March to June of 2015 at the Georgia Institute of Technology, *D. intermedius* trials were performed during June and July of 2015 at the Georgia Institute of Technology, and trials of *C. vulgaris* were performed at Arizona State University during January and February of 2015. Further details for the operation of ORPs is presented in McGowen et al.[16].

The biological growth model, for both ORP and VFP PBR, was validated against experimental data by comparing the final concentration at the end of an experimental trial period with the model result concentration for that same trial period. Meteorological data measured at the experimental site was inputted into the model in order to calculate culture light conditions. Weather data collection at experimental sites occurred at 15 minute time-intervals, therefore the models were run with 15 minute time-steps. Inorganic nutrients (carbon, nitrogen and phosphorous), besides light, were provided to not limit algal growth rates and are described in the Appendix. Culture temperature measured during the experimental trial provided the temperature input to the growth model so that any error from the thermal model would not propagate to algal productivity results. At the beginning of each comparison period, the model was initialized with the measured concentration of the experimental growth system. In each experimental comparison, light was assumed to be the primary limiting input to photosynthesis,

rather than other nutrients such as inorganic carbon, nitrogen, and phosphorous. Nutrients were provided in excess of requirements for the cultivation period used for productivity assessment. A nutrient depletion phase was avoided to enhance lipid content. Moreover, the pH in each trial was maintained in a range that did not affect algal growth rates. For ATP[3] experimental trials, this was a range between 7.0 and 8.0, for experimental work with *G. sulphuraria* pH 2.5 was used (buffered by $H_3PO_4/H_2PO_4^{-}$) to accommodate the algae's acidophilic nature [16,17,24]. Finally, supplemental CO_2 and oxygen content of greater than 30% within the cultures maximized algal growth dynamics. At the end of each comparison period, the modeled biomass concentration was compared to the experimentally measured biomass concentration. Formulas for the error values computed in this study and a typical plot of concentration as a function of time for a VFP array are shown in the Appendix.

Case Study Methods

To demonstrate the capability of this model to predict algal productivity at various locations, three sites were chosen as case study locations; Baton Rouge LA, Fort Collins CO, and Scottsdale, AZ. Model results for one year were calculated at each location with strain characteristics for *Galdieria sulphuraria 5587.1* and *Chlorella vulgaris* in an array of VFP PBRs and an array of ORPs respectively. These strains were evaluated based on their promising potential as biofuel feedstock. In each case, the models were initialized at 100 g m^{-3} and set to harvest when concentration reached 300 g m^{-3}. Though VFP PBRs may be operated at much higher concentrations than the 100 g m^{-3} and 300 g m^{-3} boundaries, the concentration boundaries were kept consistent between methodologies to illustrate that the model can illuminate differences in productivity between different growth architectures [16,35]. In each case study, nutrient quantities other than light were considered to not limit growth rates. The net harvested

mass, summed for the entire year, is the total biomass productivity of the system based on the harvest outlined above. Weather data was gathered from the NREL TMY3 dataset [36]. Other model inputs for these specific case studies are summarized in the Appendix.

RESULTS AND DISCUSSION

Results are divided into three sections, 1) model validation across multiple strains and reactor configurations, 2) model sensitivity, and 3) application of the model for the evaluation of performance of strains in different reactor configurations and locations. The successful validation of each of the several combinations of algal strain and system geometry contributes to overall confidence in the model.

Thermal Model Validation

Temperature has been shown to be a critical variable impacting algal productivity [17,23,24,37,38]. The two types of systems evaluated were a VFP PBR and ORP. A comparison of the model calculated and experimentally measured temperature of the middle 3rd vertical flat panel, in an array of 6 total VFP PBRs, facing east-west normal was performed. Figures illustrating the accuracy of each thermal model are available in the Appendix. Average accuracy for the models are 2.7 K with a standard deviation of 1.8 K. and 1.5 K with a standard deviation of 0.98 K for the VFP PBR and ORP, respectively.

An acceptable error in this model is based on comparison with similar studies and uncertainties in weather data. For instance, the thermal model accuracy is consistent with values reported in the literature such as Bechet et al.[34,34] which reported an accuracy of 2.4 K and 1.5 K respectively. Moreover, the accuracy reported in Bechet et al.[31] for prediction of a closed PBR was developed from a validation period of 12 hours compared to the 14 day validation period for VFP model comparison used in this study. Considering that the optimal temperature is beyond the top 8 most sensitive parameters to model output algal concentration for both the VFP PBR and ORP, the margin of error in temperature prediction is acceptable. Distinguishing the scope of

this study from other, more limited studies, such as Endres et al.[7] is the coupling of the thermal model to a robust biological growth model.

Biological Model Validation

Vertical Flat Panel Growth Model Validation

The model developed in this paper was evaluated through the ability to predict algal concentration in a real, outdoor system. The validation of the model for VFP PBR was performed through modeling growth at the AzCATI facility and comparing results to experimental data. Primary inputs of meteorological data and operating conditions of the experimental trials for an east-west facing array of VFP PBRs were inputted into the model. Contamination of the algal biomass observed in these experimental trials was minimal. A comparison between modeled final concentration of algal biomass and experimental concentration of algal biomass for four trials of *G. sulphuraria* 5587.1 occurring in the summer of 2016 at AzCATI is summarized in Figure 1a. The average error among the four trial results shown is ±11.8% with a standard deviation of 8.9%. The model does not consistently over or under predict algal concentration sugesting the error is related to biologal inconsistencies. Considering the broad range of inputs that the model accepts, the model accurately considers the physical parameters with the most emphatic effect on biomass productivity of a VFP PBR. Validation at a smaller timescale with *G. sulphuraria Soos* indicates that the model is an effective continous representation of algal concentration, as shown in Figure 2. An average accuracy of 3.3% was observed during a weeklong trial of photoautotrophic growth of *G.*

sulphuraria Soos with a standard deviation of 3%.

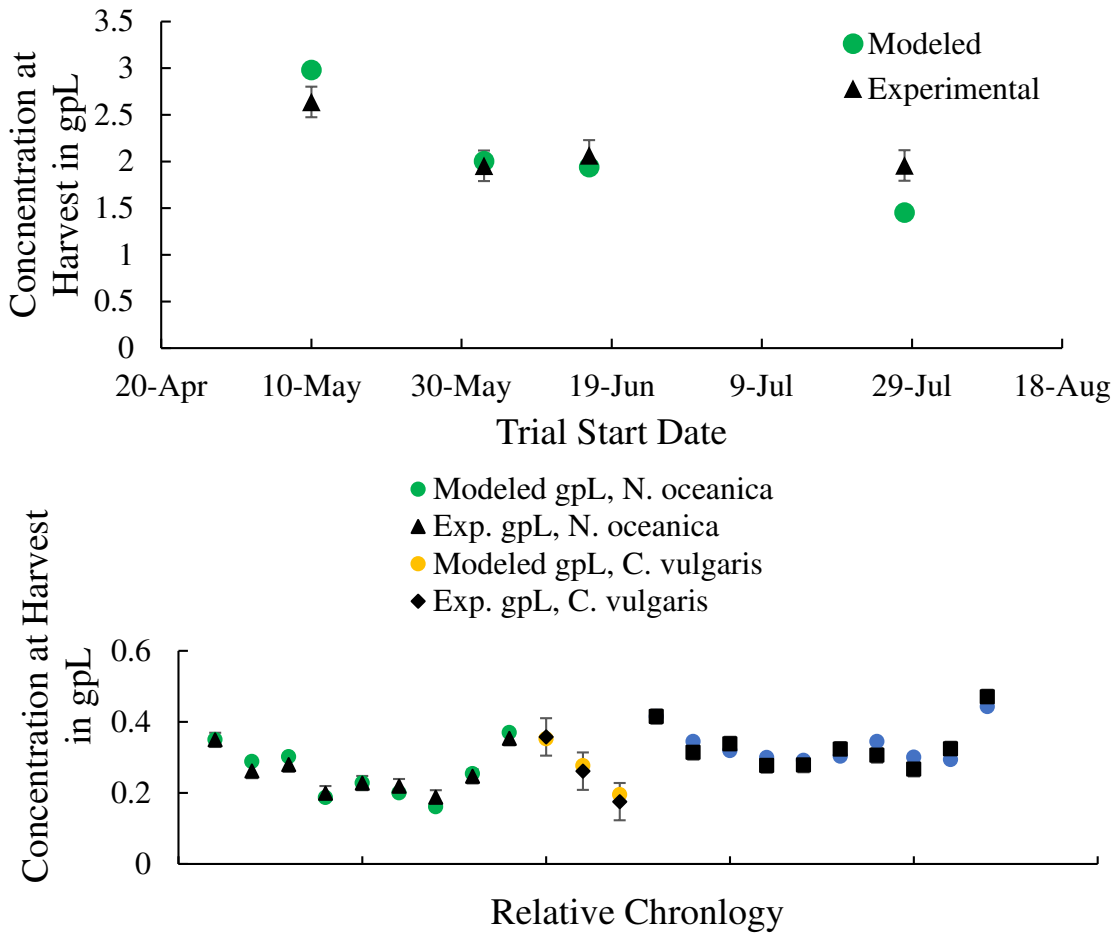

Figure 1: A) Validation plot comparing model results for final concentration to experimental results for final concentration of Galdieria sulphuraria grown in VFP PBRs at AzCATI in 2016. Trials typically lasted between 1 and 3 weeks. The average error among the 4 trial results is ±11.8%. Values shown are for an average of 4 units with error bars representing the standard deviation for individual VFP PBRs in an array facing east to west. B) A condensed plot showing a comparison between model and experimental final trial concentrations of algal biomass for 3 algae strains grown as a part of the ATP[3] testbed project. Each concentration value expressed is the average of 6 ORPs with error bars representing the standard deviation. Across the 22 trials evaluated, there is an average error of 6.7%.

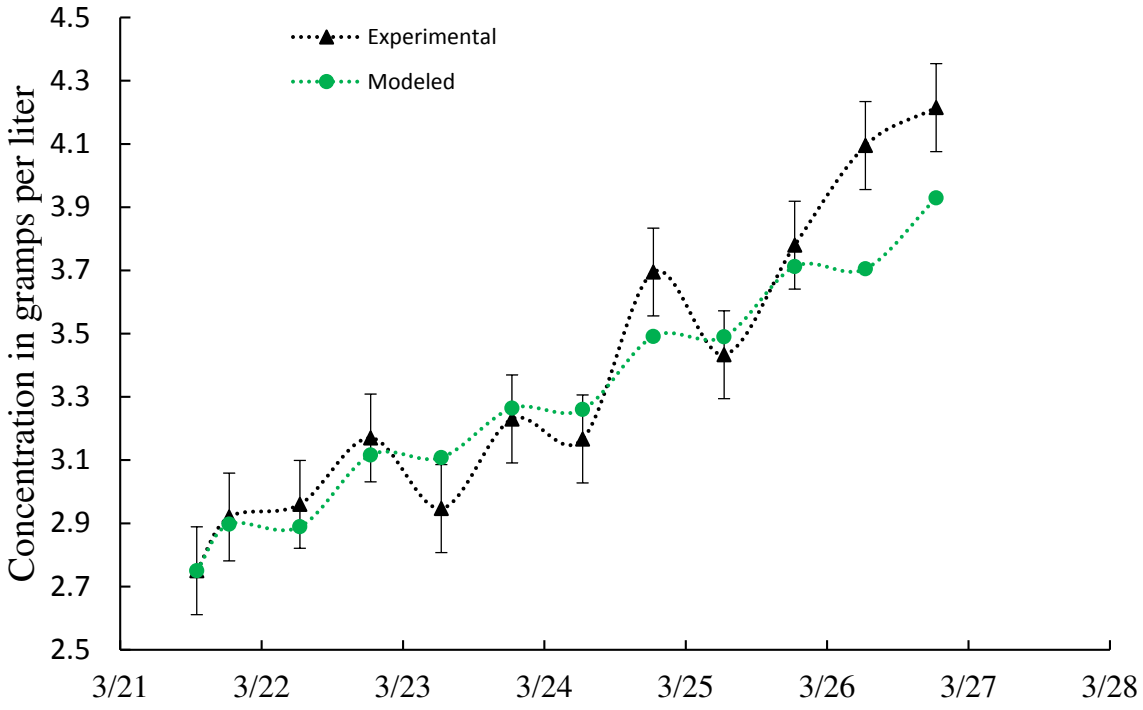

Figure 2: Comparison of model predicted vs. average measured concentration of algal biomass in the interior 4 panels of an array of 6 VFP PBRs, facing east-west normal. The experimental data was developed at AzCATI with G. sulphuraria Soos over one week in March 2017. Average error is 3.3% with a standard deviation of 3%. Error bars indicate the standard error for the experimental data set.

Open Raceway Pond Growth Model Validation Results

The growth model was adapted to ORP architecture and validated in a similar fashion to the VFP PBR. Metrological data, strain characterization, and reactor architecture inputs were used to predict growth in ORPs and compared to experimental results. Summarized in Figure 1b, is a comparison between model and experimental results for 22 trials, and three different algae strains from the ATP[3] test sites, at the Georgia Institute of Technology (*Nannochloropsis oceanica* and *Desmodesmus intermedius)* and AzCATI (*C. vulgaris)*. All trials used for validation showed minimal contamination. Each experimental value shown is an average of the final concentration for 6 individual ORPs. Across the 22 trials compared, there is an average error of ±6.7% with a standard deviation of 5.33%.

The *Nannochloropsis oceanica* experimental trials were performed at the Georgia Institute of Technology from May 12th to June 15th of 2015. The modeling accuracy of these trials displayed an average error of 6.2% with a standard deviation of 7%. The *Chlorella vulgaris* trials were performed at AzCATI during January through February of 2015 with an average error of 6.2% between model and experimental biomass concentration with a standard deviation of 5%. The *Desmodesmus intermedius* experimental trials that were performed at the Georgia Institute of Technology during June and July of 2015 display an average error of 7.5% between model and experimental biomass concentration with a standard deviation of 3.0%. Similar to the validation results for model application to VFP PBRs, the open raceway pond model does not consistently over- or under-predict the trial conclusion of algal biomass concentrations. The consistency of this trend across both architectures, and several different strains of microalgae, suggests that the model accurately captures the key physical parameters effecting algal biomass growth.

Comparison to model accuracy in existing literature

Significant investments exist in developing algal growth models. Bechet et al.[10], Cornet and Dussap[39], Fernandez et al.[40], and Quinn et al.[12] developed and validated growth models focused on closed PBR based systems. The accuracy of modeling efforts have continually improved from the work of Fernandez et. al[40] which was shown to predict productivity to within 20%. Subsequent work by Bechet et al.[10] and Quinn et al.[12] predicted end biomass concentration to 8.4% and 9.2% accuracy, respectively. While the models by Bechet et al.[10] and Quinn et al.[12] were accurate, their applicability was restrictive as the models developed were limited to predicting growth in a fixed architecture. Cornet and Dussap[39] sought to develop a model with expanded applicability and accuracy. However, their model that showed ±8.1% average

accuracy, was validated against varying reactor geometries with controlled light conditions in an indoor setting, providing minimal confidence to any implementation of that model in outdoor settings. The model developed in this study reproduces accuracy comparable to preexisting models of closed algal growth systems with the ability to model other growth geometries as well.

Other modeling efforts have focused on the development of ORP growth models but with many of them lacking validation [13,14,41]. Early bulk growth modeling by Guterman[42] developed a model of growth in an outdoor pond and compared it to experimental results with accuracy of ±20.2. Recently, Huesemann et al.[43] developed an outdoor ORP model that demonstrated an ability to predict biomass productivity under semi-continuous conditions. The model developed by Huesemann et al.[43] requires similar key parameters to this model, optimum temperature, optimum incident light intensity, and night respiration rate. However, Huesemann et al.[43] relies on values for each of the strain descriptive input parameters being established from a continuous range or through multivariable variation. Though the respiration biomass loss rate input to this model is empirically derived, it is the 4th least sensitive model parameter of those tested for both VFPs and ORPs. This study seeks to address the need for a robust bulk growth model that requires minimal strain characterization data and can support sustainability assessments. Several techno-economic and life-cycle analysis identify ORPs as the principle growth architecture, which demonstrates the utility of an accurate, validated growth model for open systems[1,44,45].

This model represents a valuable platform for a variety of analytical exercises that could evaluate algal growth systems at various locations prior to experimental trials. Moreover, the parameterization resulting from a finished model enables optimization and geographic resource assessment. Compared to Bechet et al[46], the model presented here provides a more relevant output since model validation performed in this study utilized outdoor, pilot-scale experimental

results, rather than indoor, bench scale. Though the accuracy in predicting growth of *G. sulphuraria* presented in Jayaraman and Rhinehart[11] is strong, the input parameters for that study were developed through a leap-frogging regression approach, rather than insight from algal strain characterization. Other modeling efforts such as Quinn et al.[12] and Moody et al.[47] have been shown to be valuable in assessing algal productivity, though the model is limited to predicting growth in the architecture leveraged for validation. Considered summarily, the model of algal growth developed in this study accomplishes two principle objectives: the modeling method is demonstrably accurate across a spectrum of cultivation scenarios and the model does not require prohibitive system characterization to provide meaningful predictive results.

Within the Appendix is a typical plot of concentration for a VFP PBR model output. Concentrations of different units within the larger array deviate from one another due to differences in temperature and irradiance as a result of shading and inter-panel reflection. This result illustrates the fidelity of the VFP PBR model towards interactions with algal growth such as interpanel-reflection and dynamic temperature profile evolution. This fidelity carries forward to more meaningful extrapolation results through coupling to datasets such as the TMY3 that will summarize weather events for a model year[36]. Furthermore, effects due to changes in reactor spacing, orientation, and solar hour are evident in the sensitivity model of VFP PBRs indicating a capability to evaluate different design scenarios using this model. The Appendix summarizes the sensitivities of these parameters.

Growth Model Sensitivities

An understanding of the effects of inherent error in model inputs is a fundamental detail impacting the boundaries of model utility. A sensitivity analysis performed for both the VFP PBR and ORP coupled thermal-growth models identifies the parameters with greatest effect on

the model. Input variables were altered by increments of ±10% to elucidate modeled biomass productivity sensitivity. A t-ratio analysis performed therein is summarized for the VFP PBR and ORP in the appendix. Comparison of these values to the critical t-ratios for a 95% confidence interval seeks to inform the model inputs for which highest accuracy is required.

The sensitivity analysis performed in this study identifies similar parameters with peak sensitivity as Quinn et al.[12] and Jayaraman and Rhinehart[11]. In all three cases, optimum and operating temperatures are statistically important to the model. The number of parameters with t-ratios beyond the 95% confidence margin reported in Quinn et al.[12] is greater than that shown in this model. The sensitivities analysis performed in Jayaraman and Rhinehart[11] yielded results more consistent with the sensitivities observed in this study. Model sensitivity t-ratios can provide an indication of how difficult developing accurate parameters for model extrapolation may be; models with many estimated parameter t-ratios exceeding the desired confidence margin will require very accurate inputs to those parameters to maintain model accuracy. Though this is a qualitative understanding of the role of sensitivity in model development, the number of sensitive variables estimated through input variation that exceed the critical t-ratio provide a quantitative means of comparison between different modeling approaches. In both the ORP and VFP PBR models developed in this study, temperature conditions and growth architecture geometric parameters have the greatest model sensitivities.

The variables with the greatest sensitivity in the VFP PBR model are ambient temperature, geometric dimensions, and spectral characteristics. Spectral characteristics may have a particularly large impact since there are numerous, distinct modes of heat transfer that are linearly affected by absorptivity and transmissivity as well as the extent of culture irradiance. Likewise, when considering PBR dimensions, the dimensions of the PBR affects nearly every

heat transfer mode, as well as the amount of solar energy absorbed in time. Ambient air temperature is significant since the panel geometry is conducive to substantial convection heat transfer with ambient air. Consequently, the input values of those sensitive metrics utilized during extrapolation of the model from this study should receive the most rigorous scrutiny.

The variables with the greatest sensitivity in the ORP model are the harvest operation inputs, geometric variables, and weather inputs. Considering that the sole means of culture irradiance for growth is direct solar irradiance, as well as the dominant mode of heat transfer in the ORP, it is not surprising that the model is relatively sensitive to GHI values. Analogously, the depth influences a linear factor of growth, the opacity efficiency, by the attenuation of light in a non-transparent culture. This relationship, considered alongside the harvest concentration, suggests that the opacity efficiency has a meaningful effect on the performance of the ORP from a biomass accumulation perspective. The sensitivity to harvest concentration may provide a platform for optimization considering harvest energy consumption. Spectral characteristics also effect the modeled concentration, though not to the extent of the VFP PBR.

In both the ORP and VFP results, the data input time-resolution maintains appropriate fidelity to fluctuating weather conditions. This is demonstrated based on the agreement between the results from model executions with input data at the 15min time scale and experimental results. Fluctuations in weather represents an important aspect to algal modeling with this model demonstrated to accurately capture these effected based on validation.

Case Studies Results

As a means of developing an understanding of the utility for the model developed in this study, full-year biomass productivity for 6 case studies was evaluated. The results are presented both as an areal productivity (g m^{-2} day^{-1}) and a volumetric productivity (g L^{-1} day^{-1}) for the

growth architecture simulated, in order to reflect productivity metrics typical of an algal biomass to biofuel process [4]. To provide a preliminary understanding of geographic effects on model results, the model was run with datasets corresponding to a typical meteorological year in Baton Rouge LA, Fort Collins CO, and Scottsdale AZ[36]. A model evaluation for *G. sulphuraria* VFP PBRs and *C. vulgaris* in ORPs was performed for each site with results summarizing the 6 case studies shown in Table 1. A qualitative review of the case study results suggests that warm temperatures and abundant solar irradiance are conducive to higher algal productivity. To further understand this effect and the interplay between temperature and irradiance relations with seasonal variability predictions from the model,calculations of average biomass productivity over a week during June (Peak) and January (Minimum) were performed for each of the case study scenarios, summarized in Table 1.

Table 1: Summary of case study results for Chlorella vulgaris grown in ORPs and Galdieria sulphuraria grown in VFP PBRs at 3 different locations in the United States. Areal and volumetric productivities were averaged over a year as well as one week in January and one week in June. The effects of seasonal variability in weather patterns on the productivity for the strains and growth architectures selected are illustrated by the differences in productivity for weeks in June and January.

Location	**Strain**	**Growth Architecture**	**Avg. Areal Biomass Productivity June 1-7 (g/m^2-day)**	**Avg. Areal Biomass Productivity Jan. 1-7 (g/m^2-day)**	**Avg. Annual Areal Biomass Productivity (g/m^2-day)**	**Avg. Annual Volumetric Productivity (g/L-day)**
Baton Rouge, LA	*C. vulgaris*	ORP	11.0	5.58	13.2	0.023
Fort Collins, CO	*C. vulgaris*	ORP	8.71	4.49	10.8	0.043
Scottsdale, AZ	*C. vulgaris*	ORP	21.6	6.24	15.6	0.062

Baton Rouge, LA	*G. sulphuraria 5587.1*	VFP PBR	9.78	3.17	7.07	0.066
Fort Collins, CO	*G. sulphuraria 5587.1*	VFP PBR	7.31	0.958	4.29	0.042
Scottsdale, AZ	*G. sulphuraria 5587.1*	VFP PBR	15.48	2.78	9.04	0.089

The effects of seasonal variability in culture conditions on biomass productivity are evident. The January average productivities drop as low as 8.6% of the June average productivities. This result emphatically suggests that an understanding of full year algal productivity must consider seasonal impacts on peak productivity. Moreover, the *G. sulphuraria* VFP model productivity suffers greater percentage reductions in productivity between summer and winter, which is primarily attributed to the high optimum culture temperature of the species, 42 °C. For instance, the results for Baton Rouge LA, the VFP PBR with *G. sulphuraria* demonstrates greater summer productivity than *C. vulgaris* in an ORP but less winter productivity. This result suggests that groups seeking practical approaches to growing algae in a climate similar to Baton Rouge should consider a hybrid approach between strains and growth architectures to maximize areal productivity.

REFERENCES

(1) Beal, C. M.; Gerber, L. N.; Sills, D. L.; Huntley, M. E.; Machesky, S. C.; Walsh, M. J.; Tester, J. W.; Archibald, I.; Granados, J.; Greene, C. H. Algal biofuel production for fuels and feed in a 100-ha facility: A comprehensive techno-economic analysis and life cycle assessment. *Algal Res.* **2015**, *10*, 266–279.

(2) Jones, S.; Zhu, Y.; Anderson, D.; Hallen, R.; Elliott, D. C.; Schmidt, A. J.; Albrecht, K.; Hart, T.; Butcher, M.; Drennan, C.; et al. Process design and economics for the conversion of algal biomass to hydrocarbons: whole algae hydrothermal liquefaction and upgrading. *US Dep. Energy Bioenergy Technol. Off.* **2014**.

(3) Barlow, J.; Sims, R. C.; Quinn, J. C. Techno-economic and life-cycle assessment of an attached growth algal biorefinery. *Bioresour. Technol.* **2016**, *220*, 360–368.

(4) Quinn, J. C.; Davis, R. The potentials and challenges of algae based biofuels: A review of the techno-economic, life cycle, and resource assessment modeling. *Bioresour. Technol.* **2015**, *184*, 444–452.

(5) Slegers, P. M.; van Beveren, P. J. M.; Wijffels, R. H.; van Straten, G.; van Boxtel, A. J. B. Scenario analysis of large scale algae production in tubular photobioreactors. *Appl. Energy* **2013**, *105*, 395–406.

(6) Slegers, P. M.; Wijffels, R. H.; van Straten, G.; van Boxtel, A. J. B. Design scenarios for flat panel photobioreactors. *Appl. Energy* **2011**, *88* (10), 3342–3353.

(7) Endres, C. H.; Roth, A.; Brück, T. B. Thermal Reactor Model for Large-Scale Algae Cultivation in Vertical Flat Panel Photobioreactors. *Environ. Sci. Technol.* **2016**, *50* (7), 3920–3927.

(8) Husselmann, A. V.; Hawick, K. A. Simulating Growth Kinetics in a Data-Parallel 3D Lattice Photobioreactor. *Model. Simul. Eng.* **2013**, *2013*, 1–10.

(9) Papáček, Š.; Matonoha, C.; Štumbauer, V.; Štys, D. Modelling and simulation of photosynthetic microorganism growth: random walk vs. finite difference method. *Math. Comput. Simul.* **2012**, *82* (10), 2022–2032.

(10) Béchet, Q.; Shilton, A.; Guieysse, B. Full-Scale Validation of a Model of Algal Productivity. *Environ. Sci. Technol.* **2014**, *48* (23), 13826–13833.

(11) Jayaraman, S. K.; Rhinehart, R. R. Modeling and Optimization of Algae Growth. *Ind. Eng. Chem. Res.* **2015**, *54* (33), 8063–8071.

(12) Quinn, J.; de Winter, L.; Bradley, T. Microalgae bulk growth model with application to industrial scale systems. *Bioresour. Technol.* **2011**, *102* (8), 5083–5092.

(13) Weyer, K. M.; Bush, D. R.; Darzins, A.; Willson, B. D. Theoretical Maximum Algal Oil Production. *BioEnergy Res.* **2010**, *3* (2), 204–213.

(14) Zemke, P. E.; Wood, B. D.; Dye, D. J. Considerations for the maximum production rates of triacylglycerol from microalgae. *Biomass Bioenergy* **2010**, *34* (1), 145–151.

(15) Laurens, L. M. L.; Van Wychen, S.; Pienkos, P. T.; Harmon, V. L.; McGowen, J. Harmonization of experimental approach and data collection to streamline analysis of biomass composition from algae in an inter-laboratory setting. *Algal Res.* **2017**.

(16) McGowen, J.; Knoshaug, E. P.; Laurens, L. M. L.; Dempster, T. A.; Pienkos, P. T.; Wolfrum, E.; Harmon, V. L. The Algae Testbed Public-Private Partnership (ATP 3)

framework; establishment of a national network of testbed sites to support sustainable algae production. *Algal Res.* **2017**, *25*, 168–177.
(17) Gross, W.; Oesterhelt, C.; Tischendorf, G.; Lederer, F. Characterization of a non-thermophilic strain of the red algal genus *Galdieria* isolated from Soos (Czech Republic). *Eur. J. Phycol.* **2002**, *37* (3), 477–482.
(18) Selvaratnam, T.; Henkanatte-Gedera, S. M.; Muppaneni, T.; Nirmalakhandan, N.; Deng, S.; Lammers, P. J. Maximizing recovery of energy and nutrients from urban wastewaters. *Energy* **2016**, *104*, 16–23.
(19) Toplin, J. A.; Norris, T. B.; Lehr, C. R.; McDermott, T. R.; Castenholz, R. W. Biogeographic and Phylogenetic Diversity of Thermoacidophilic Cyanidiales in Yellowstone National Park, Japan, and New Zealand. *Appl. Environ. Microbiol.* **2008**, *74* (9), 2822–2833.
(20) Lomax, H.; Pulliam, T. H.; Zingg, D. W. *Fundamentals of Computational Fluid Dynamics*, 2nd ed.; Scientific Computation; Springer-Verlag: Berlin, 2003.
(21) Wilhelm, C.; Jakob, T. From photons to biomass and biofuels: evaluation of different strategies for the improvement of algal biotechnology based on comparative energy balances. *Appl. Microbiol. Biotechnol.* **2011**, *92* (5), 909–919.
(22) Alexandrov, G. A.; Yamagata, Y. A peaked function for modeling temperature dependence of plant productivity. *Ecol. Model.* **2007**, *200* (1–2), 189–192.
(23) Geider, R., J.; Osborne, B. A. *Algal Photosyntehsis*; Current Phycology; 1992.
(24) Oesterhelt, C.; Schmälzlin, E.; Schmitt, J. M.; Lokstein, H. Regulation of photosynthesis in the unicellular acidophilic red alga Galdieria sulphuraria†: Regulation of photosynthesis in Galdieria. *Plant J.* **2007**, *51* (3), 500–511.
(25) Contreras, A.; Garcia, F.; Molina, E.; Merchuk, J. C. Interaction Between CO2-Mass Transfer, Light Availability, and Hydrodynamic Stress in the Growth of Phaeodactylum tricornutum in a Concentric Tube Photobioreactor. *Biotechnol. Bioeng.* **1998**, *60* (3), 317–325.
(26) Marshall, J. S.; Sala, K. A stochastic Lagrangian approach for simulating the effect of turbulent mixing on algae growth rate in a photobioreactor. *Chem. Eng. Sci.* **2011**, *66* (3), 384–392.
(27) Molina, E.; Fernández, J.; Acién, F. G.; Chisti, Y. Tubular photobioreactor design for algal cultures. *J. Biotechnol.* **2001**, *92* (2), 113–131.
(28) Yuan, S.; Zhou, X.; Ochieng, R. M.; Zhou, X. A numerical thermal growth model for prediction of microalgae production in photobioreactors. *J. Renew. Sustain. Energy* **2016**, *8* (2), 023102.
(29) Singh, S. P.; Singh, P. Effect of temperature and light on the growth of algae species: A review. *Renew. Sustain. Energy Rev.* **2015**, *50*, 431–444.
(30) Zhang, K.; Kurano, N.; Miyachi, S. Outdoor culture of a cyanobacterium with a vertical flat-plate photobioreactor: effects on productivity of the reactor orientation, distance setting between the plates, and culture temperature. *Appl. Microbiol. Biotechnol.* **1999**, *52* (6), 781–786.
(31) Béchet, Q.; Shilton, A.; Fringer, O. B.; Muñoz, R.; Guieysse, B. Mechanistic Modeling of Broth Temperature in Outdoor Photobioreactors. *Environ. Sci. Technol.* **2010**, *44* (6), 2197–2203.
(32) Goetz, V.; Le Borgne, F.; Pruvost, J.; Plantard, G.; Legrand, J. A generic temperature model for solar photobioreactors. *Chem. Eng. J.* **2011**, *175*, 443–449.

(33) Bergman, T. L.; Lavine, A. S.; Incropera, F. P.; Dewitt, D. P. *Fundamentals of Heat and Mass Transfer*, 7th ed.; John Wiley & Sons, Inc., 2011.
(34) Béchet, Q.; Shilton, A.; Park, J. B. K.; Craggs, R. J.; Guieysse, B. Universal Temperature Model for Shallow Algal Ponds Provides Improved Accuracy. *Environ. Sci. Technol.* **2011**, *45* (8), 3702–3709.
(35) Münkel, R.; Schmid-Staiger, U.; Werner, A.; Hirth, T. Optimization of outdoor cultivation in flat panel airlift reactors for lipid production by Chlorella vulgaris. *Biotechnol. Bioeng.* **2013**, *110* (11), 2882–2893.
(36) Wilcox, S.; Marion, W. *Users manual for TMY3 data sets*; National Renewable Energy Laboratory Golden, CO, 2008.
(37) Sandnes, J. M.; Källqvist, T.; Wenner, D.; Gislerød, H. R. Combined influence of light and temperature on growth rates of Nannochloropsis oceanica: linking cellular responses to large-scale biomass production. *J. Appl. Phycol.* **2005**, *17* (6), 515–525.
(38) Vanags, J.; Kunga, L.; Dubencovs, K.; Galvanauskas, V.; Grīgs, O. Influence of Light Intensity and Temperature on Cultivation of Microalgae Desmodesmus Communis in Flasks and Laboratory-Scale Stirred Tank Photobioreactor. *Latv. J. Phys. Tech. Sci.* **2015**, *52* (2), 59–70.
(39) Cornet, J.-F.; Dussap, C.-G. A simple and reliable formula for assessment of maximum volumetric productivities in photobioreactors. *Biotechnol. Prog.* **2009**, *25* (2), 424–435.
(40) Fernandez, F. G.; Camacho, F. G.; Perez, J. A.; Sevilla, J. M.; Grima, E. M. Modeling of biomass productivity in tubular photobioreactors for microalgal cultures: effects of dilution rate, tube diameter, and solar irradiance. *Biotechnol. Bioeng.* **1998**, *58* (6), 605–616.
(41) Wigmosta, M. S.; Coleman, A. M.; Skaggs, R. J.; Huesemann, M. H.; Lane, L. J. National microalgae biofuel production potential and resource demand: NATIONAL ALGAE BIOFUEL PRODUCTION. *Water Resour. Res.* **2011**, *47* (3), n/a-n/a.
(42) Guterman, H.; Vonshak, A.; Ben-Yaakov, S. A macromodel for outdoor algal mass production. *Biotechnol. Bioeng.* **1990**, *35* (8), 809–819.
(43) Huesemann, M.; Crowe, B.; Waller, P.; Chavis, A.; Hobbs, S.; Edmundson, S.; Wigmosta, M. A validated model to predict microalgae growth in outdoor pond cultures subjected to fluctuating light intensities and water temperatures. *Algal Res.* **2016**, *13*, 195–206.
(44) Béchet, Q.; Shilton, A.; Guieysse, B. Maximizing Productivity and Reducing Environmental Impacts of Full-Scale Algal Production through Optimization of Open Pond Depth and Hydraulic Retention Time. *Environ. Sci. Technol.* **2016**, *50* (7), 4102–4110.
(45) Davis, R.; Markham, J.; Kinchin, C.; Grundl, N.; Tan, E. C.; Humbird, D. Process Design and Economics for the Production of Algal Biomass: Algal Biomass Production in Open Pond. **2016**.
(46) Béchet, Q.; Chambonnière, P.; Shilton, A.; Guizard, G.; Guieysse, B. Algal productivity modeling: A step toward accurate assessments of full-scale algal cultivation. *Biotechnol. Bioeng.* **2015**, *112* (5), 987–996.
(47) Moody, J. W.; McGinty, C. M.; Quinn, J. C. Global evaluation of biofuel potential from microalgae. *Proc. Natl. Acad. Sci.* **2014**, *111* (23), 8691–8696.

APPENDIX I: SUPPLEMENTARY INFORMATION

Stoichiometry for conversion factor, φ

Considering full cycle photosynthesis summarized as [1], with Carbon having a molecular mass of 12.01 g/mol,

$$CO_2 + H_2O + (8 - 10\ Photons\ per\ O_2) \leftrightarrow\ CH_2OXX + O_2 \qquad [1]$$

And the assumption that biomass is approximately 50% carbon Quinn et al.[1], a value for $\emptyset_{photon}$ of approximately 12/18 (midpoint between 12/16 and 12/20) is obtained. CH_2OXX is a generalized expression of a hydro-carbon molecule, summarizing the fact that the macromolecular results of photosynthetic metabolism vary[2].

$$\emptyset_{photon} = \frac{12\ Carbon}{18\ Photons} \qquad [2]$$

$$P = C1 \cdot \sum I_n \qquad [3]$$

Where $\emptyset_{photon}$ is the carbon to photon conversion factor, P is the rate of photosynthetic spectrum photon incidence in μE/m^2*s, C1 is a constant equal to 4.56e-6 mol PAR photons per Joule blackbody radiation, and $\sum I_n$ is the sum of incident sources of radiation in joules.

Methodology for determining respiration rate

Recall the governing equation for biomass concentration as a function of time from the manuscript of this study:

$$\frac{dC_x}{dt} = \frac{\varphi_L \cdot \varphi_T \cdot \varphi_C \cdot P \cdot \emptyset_{photon}}{V} - D/V \qquad [2]$$

Where D is the decay rate in grams biomass per grams biomass-second

$$D = \varphi_L \cdot \varphi_T \cdot \emptyset_{respiration} \qquad [3]$$

And φ_L& φ_T are the light-intensity related efficiency and temperature related efficiency respectively. The $\emptyset_{respiration}$ term is determined empirically by minimizing the difference in final biomass concentration between experimental results and the model for the $\emptyset_{respiration}$ term under adjustment. That value was determined from a single trial within the larger validation set and are summarized in Table 2.

Table 2: Respiration Biommass Loss Values Used in the Model

Strain	Respiration Value $\mu g_{biomass}\ g^{-1}\ s^{-1}$ "β"
Chlorella vulgaris	186
Galdieria sulpharia	682
Nannochloropsis oceanica	1016.8

Each value in Table 2 is converted to biomass consumed per biomass alive via the following equation:

$$\emptyset_{respiration} = \beta \cdot C_x \cdot V \qquad [5]$$

Vertical Flat Panel Heat Fluxes

Direct Irradiance

Direct irradiance of the vertical flat panels is calculated dynamically based on weather conditions and sun angles. An illustration with pertinent dimensions is shown in Figure 3.

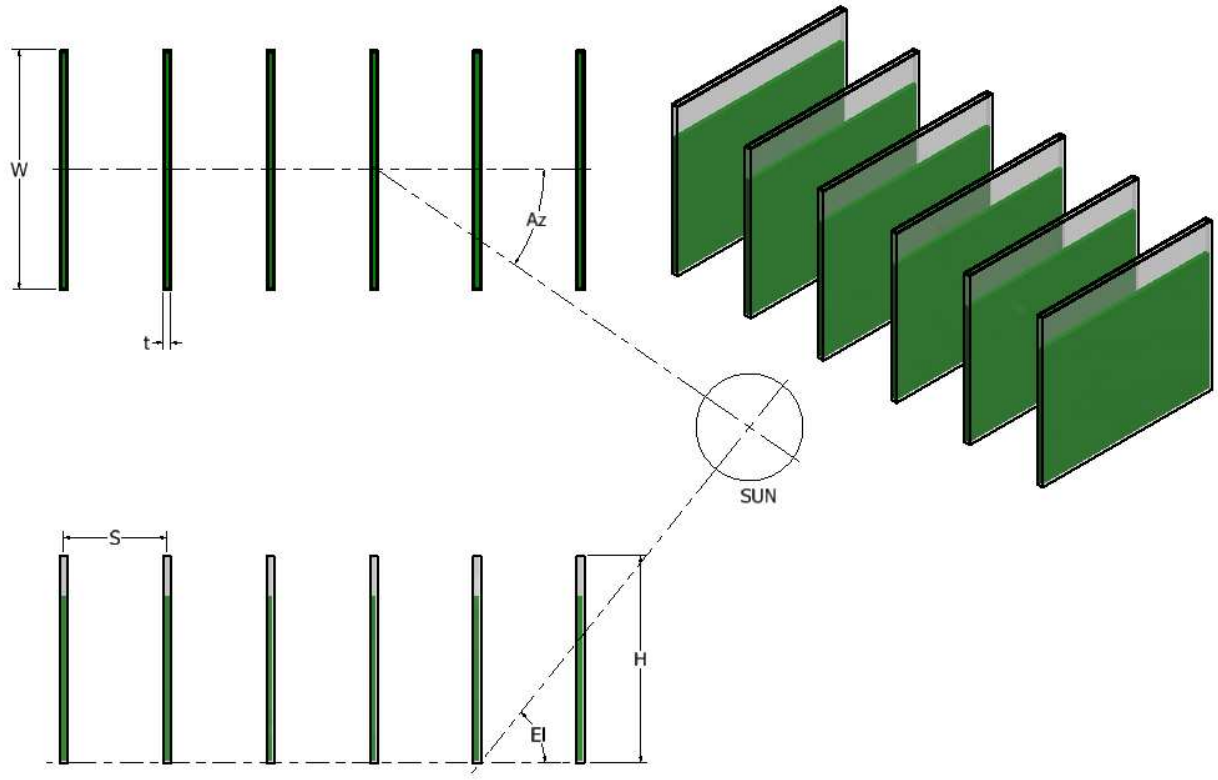

Figure 3: Diagram showing critical dimensions of VFP PBR

Direct solar irradiance is calculated as follows:

$$Q_{direct} = DNI \cdot \alpha \cdot \tau \cdot A' \cdot \cos(\delta) \qquad [6]$$

Where DNI is direct normal irradiance (W m^{-2}), α is spectral absorptivity, τ is the transmissivity of the VFP material, A' is the critical area, and δ is the angle between a vector orthogonal to the vertical face of the PBR and the sun. The formula for A' is calculated as follows, building on the method developed by Slegers et al.[3] and Endres[4]:

$$W' = S \cdot \tan(Az) \qquad [7]$$

$$H' = S \cdot \tan(El) \qquad [8]$$

$$A' = H' \cdot W' \qquad [9]$$

In this study, the compass orientation is a user input. Therefore, δ must be determined more rigorously according to the following process.

With γ the compass orientation of a vector normal to the face of a panel, varying from 0 to 2 π radians, clockwise:

$$V1 = |\sin(\gamma) \quad \cos(\gamma) \quad 0| \qquad [10]$$

$$V2 = |\sin(Az) \quad \cos(Az) \quad \sin(El)| \qquad [11]$$

$$\delta = \arccos(V1 * V2) \qquad [12]$$

Where $*$ designates the dot product of two vectors. Since V1 and V2 are unit vectors, the magnitude term traditional in calculations similar to eq. 12 has been omitted.

Diffuse Irradiance

The heat flux contribution due to diffuse solar irradiance of a vertical flat panel PBR is calculated as follows, building on the methodology presented by Slegers et al.[3] and Endres et al.[4]:

$$Q_{diffuse} = 2 \cdot DHI \cdot \alpha \cdot \tau \cdot F1 \cdot A \qquad [13]$$

F is the view factor correlation from Howell et al.[5]:

$$F1 = \frac{1}{2} \cdot \left(1 + \frac{H}{S} - \sqrt{1 + \left(\frac{H}{S}\right)^2}\right) \qquad [14]$$

Where h is the panel height, s is the spacing between panels, A is the area of one full panel face, and DHI is the diffuse horizontal irradiance. Note that the expression $DHI \cdot \alpha \cdot \tau \cdot F1 \cdot A$ is multiplied by 2 to account for both sides of one VFP PBR.

Distant Atmospheric Irradiance

The heat flux contribution due to distant, longwave, atmospheric irradiance of a vertical flat panel PBR is calculated as follows, building on the methodology presented by Slegers et al.[3] and Endres et al.[4].

$$Q_{atmo} = F1 \cdot \varepsilon_{sky} \cdot \sigma \cdot T_{sky}^4 \cdot \alpha \cdot \tau \cdot 2 \cdot A \qquad [15]$$

$$T_{sky}^1 = \left(\varepsilon_{sky} \cdot T_{amb}^4\right)^{1/4} \qquad [16]$$

Ground Irradiance

The heat flux contribution due to radiation emanating from the ground is calculated as follows, building on the methodology presented by Bechet et al.[6], Slegers et al.[3] and Endres et al.[4]:

$$Q''_{ground} = \sigma \cdot \varepsilon_{grnd} \cdot T_{grnd}^4 \cdot F1 \cdot \alpha \cdot \tau \qquad [17]$$

Determining the ground temperature, T_{grnd}, is a laborious process that ultimately requires a time integrated energy balance of its own. The ground temperature at a reference depth and assumed constant temperature is designated $T_{grnd\_ref} \approx 55\ °F$. The reference depth in this case was assumed 2.6 meters. A transient energy balance for the surface layer is configured as

$$\frac{dT_{grnd}}{dt} \cdot \rho \cdot Cp \cdot V = A_g \cdot GHI \cdot \alpha_g - Q_{conv_{grnd}} - Q_{cond_{grnd}} - Q_{radg} + Q_{atmo\_g} \qquad [18]$$

$$Q_{conv\_grnd} = \left(T_{grnd} - T_{amb}\right) \cdot h \cdot A_g \qquad [19]$$

$$Q_{cond\_grnd} = k\left(T_{grnd} - T_{grnd,n-1}\right) \cdot th^{-1} \cdot A_g \qquad [20]$$

$$Q_{radg} = \sigma \cdot \varepsilon_g \cdot T_g^4 \cdot A_g \qquad [21]$$

$$Q_{atmo\_g} = \varepsilon_{sky} \cdot \sigma \cdot T_{sky}^4 \cdot A_g \cdot \alpha_g \qquad [22]$$

$$th = \rho \cdot Cp \cdot V$$

The term h in the equation for ground convection is calculated according to the following two convection correlations from Bergman et al.[7]:

$$h = \frac{k \cdot Nu}{L} \qquad [23]$$

$$Nu = 0.54 \cdot Ra^{\frac{1}{4}} \qquad [24]$$

Or in cases of ground cooled by convection

$$Nu = 0.52 \cdot Ra^{\frac{1}{5}} \qquad [25]$$

Where Ra is the dimensionless Rayleigh number and Nu is the dimensionless Nusseldt number. Equation 18 is integrated numerically in time via an explicit, first-order, numerical integration scheme [8].

Ground Reflection

The heat transfer contribution from incident solar irradiance reflected by the ground and absorbed by a VFP panel PBR is calculated as follows [3,4]:

$$Q_{ground\_reflected} = \left(A'_g \cdot DHI \cdot \frac{\vartheta}{A} + DNI \cdot \vartheta \cdot \frac{A''_g}{A}\right) \cdot \alpha \cdot \tau \cdot A \cdot F1 \quad [26]$$

Where the term A''_g =0 for $H' < H$, $A''_g = S \cdot W \cdot \frac{H'-H}{H}$, and $A'_g = (N \cdot s * W) - (N \cdot d \cdot W)$.

Inter-panel Reflection

The heat transfer components considered reflected from one panel to another in this study are direct solar irradiance, diffuse solar irradiance, long-wave atmospheric irradiance, and ground reflection. Though theoretically other modes of irradiance are reflected, the validation process

undertaken in this study suggested that they are not relevant to a realistic concept of interpanel heat transfer. Therefore, the following summarizes the interpanel heat transfer considered in this study [3,4]:

$$Q_{reflection} = I_{dir_{ref}} + I_{diff_{ref}} + I_{atmo_{ref}} + I_{grnd_{ref}} \quad [27]$$

$$I_{dir_{ref}} = A' \cdot DNI \cdot \cos(\delta) \cdot \vartheta \cdot \tau \cdot (1-\tau) \cdot \alpha \text{ for } H' \leq \frac{H}{2} \quad [28]$$

$$I_{dir_{ref}} = F2 \cdot (H - H') \cdot W' \cdot DNI \cdot \cos(\delta) \cdot \vartheta \cdot \tau \cdot (1-\tau) \cdot \alpha \text{ for } \frac{H}{2} < H' < H \quad [29]$$

$$I_{dir_{ref}} = 0 \text{ for } H' < H \quad [30]$$

$$I_{diff_{ref}} = K \cdot F1 \cdot DHI \cdot \vartheta \cdot \alpha \cdot \tau \cdot F2 \cdot s \cdot d \quad [31]$$

Where K=1 for end panels and 2 for interior panels, of an array.

$$I_{atmo_{ref}} = K \cdot F1 \cdot \varepsilon_{sky} \cdot \sigma \cdot T_{sky}^4 \cdot A \cdot \vartheta \cdot \alpha \cdot \tau \cdot F2 \quad [32]$$

$$I_{grnd_{ref}} = K \cdot Q''_{ground} \cdot A \cdot \vartheta \cdot F2 + K \cdot Q_{ground\_reflected} \cdot \vartheta \cdot F2 \quad [33]$$

In each instance where F2, the view factor between panels facing one another appears, it is calculated with the following correlation provided from Howell et al.[5]

$$Y = H - H' \quad [34]$$

$$X = W - W' \quad [35]$$

$$G1 = \ln\left(\frac{\left((1+X^2)+(1+Y^2)\right)}{1+X^2+Y^2}\right) \quad [36]$$

$$G2 = X \cdot (1+Y^2)^{\left(\frac{1}{2}\right)} \cdot \tan^{-1}\frac{X}{(1+y^2)^{1/2}} \quad [37]$$

$$G3 = Y \cdot (1 + X^2)^{\left(\frac{1}{2}\right)} \cdot \tan^{-1}\frac{Y}{(1+X^2)^{1/2}} - X\tan^{-1}X - Y\tan^{-1}Y \quad [38]$$

$$F2 = \frac{2}{\pi XY} \cdot (G1 + G2 + G3) \quad [39]$$

Inter-panel Radiation

Contributions to the transient energy balance from reradiation by panels within the array, received by adjacent panels is calculated as follows [3,4,7]:

$$Q_{interpanel} = \sigma \cdot \varepsilon \cdot T^4 \cdot A \cdot K \cdot F2 \cdot \alpha \cdot \tau^2 \quad [41]$$

Similarly, the radiation leaving each panel is calculated as

$$Q_{reradiation} = \sigma \cdot \varepsilon \cdot T^4 \cdot A \cdot 2 \quad [42]$$

Forced and natural convection

Contributions to the transient energy balance from convection with ambient air are summarized below [3,4,7]:

$$Q_{convec} = 2 \cdot h \cdot A \cdot (T_{amb} - T) \quad [43]$$

The value for h is determined according to the following process, beginning with a velocity adjustment due to ground proximity developed by Justus and Mikhail[9]

$$n = \frac{0.37 - 0.881 \cdot \log(V_{wind})}{\left(1 - 0.0881 \cdot \log\left(\frac{hr}{10}\right)\right)} \quad [44]$$

$$c_h = \left(\frac{hr}{10}\right)^n \quad [45]$$

$$V' = c_h \cdot V_{wind} \quad [46]$$

Where V_{wind} is the wind velocity in m s^{-1} and hr is the reactor center height above the ground. A determination based on $\frac{Gr}{ReL^2}$ is made to distinguish whether conditions dictate a forced dominant or natural dominant convection process. For a $\frac{Gr}{ReL^2} < 1$ a forced dominant condition is assumed where the following Nusseldt number correlation was selected [7]:

$$NuL = 0.680 \cdot ReL^{\frac{1}{2}} \cdot Pr^{\frac{1}{3}} \quad [47]$$

Where ReL is the dimensionless Reynold's number calculated with the width of the reactor and component of V' aligned parallel to the midplane of a VFP in the array and Pr is the dimensionless Prandtl number. In cases where $\frac{Gr}{ReL^2} > 1$ a natural dominant convection regime is assumed with the following Nusseldt number correlation selection [7]:

$$NuL = \left(\frac{\left(0.825 + 0.387 \cdot RaL^{\left(\frac{1}{6}\right)}\right)}{\left(1 + \left(\frac{0.492}{Pr}\right)^{\frac{9}{16}}\right)^{\frac{8}{27}}} \right)^2 \quad [48]$$

In either case, the final h is determined via:

$$h = NuL \cdot \frac{K}{L} \quad [49]$$

Where K is the conductivity of air and L is the width of the VFP.

Evaporation

Evaporation at the surface of the water-algae mixture column within the VFP is understood to have a cooling effect on the lumped thermal mass of the VFP system. Accordingly this cooling effect is quantified according to the following process, adapted from Murphy and Berberoglu[10] and Bergman et al.[7]:

$$NuM = 0.54 \cdot RaL^{\left(\frac{1}{4}\right)} \text{ for } RaL < 10^7 \qquad [50]$$

$$NuM = 0.15 \cdot RaL^{\left(\frac{1}{3}\right)} \text{ for } RaL \geq 10^7 \qquad [51]$$

$$Sh = \frac{NuM}{Pr} \cdot Sc^{\frac{1}{3}} \qquad [52]$$

$$h_m = Sh \cdot \frac{D}{L} \qquad [53]$$

Where Sh is the dimensionless Sherwood number, Sc is the dimensionless Schmidt number, $\frac{D}{L}$ is the quotient of mass diffusivity over characteristic length, in this case the width of the VFP PBR. The mass flux of evaporated water is then calculated according to:

$$M'' = h_m \cdot (\omega_w - \omega_{air}) \qquad [54]$$

Where ω_w & ω_{air} are the mass concentrations of water vapor at the fluid-air interface and in ambient air respectively. The cooling effect due to this process, as well as convective heat rejection from the water surface, is considered via the following relation:

$$Q_{convec}II = M'' \cdot t \cdot W \cdot h_{fg} + (T_{amb} - T) \cdot NuM \cdot \frac{k}{W} \cdot t \cdot W \qquad [55]$$

where h_{fg} is the heat of vaporization of water. Similarly the cooling effect due to dry, ambient air addition as sparge gas is calculated as:

$$Q_{bubble} = M''_{air}\, h_{fg} \cdot (\omega_w - \omega_{air}) \qquad [56]$$

Under the assumption that sparge gas leaving the VFP control volume leaves as saturated air and M''_{air} is the mass-flowrate of sparge gas entering the system. The dynamic volume of culture within the VFP due to evaporative loss and subsequent addition is accounted for via:

$$V_{n+1} = V_n - \frac{M''}{\rho} \cdot dt \qquad [57]$$

Where V_{n+1} designates the volume at the next time step. During the case studies performed with the VFP model, the volume was reset to the initial culture volume every 18 hours or when the culture volume diminished below 90% of the initial culture volume, whichever happened first, to simulate dilution of the culture.

Summary and comparison of flux magnitudes

Presented in Figure 4 is a summary of the relative heat transfer contributions for each of the heat transfer modes summarized for a VFP PBR. The dominance of solar irradiance and ground radiation is apparent.

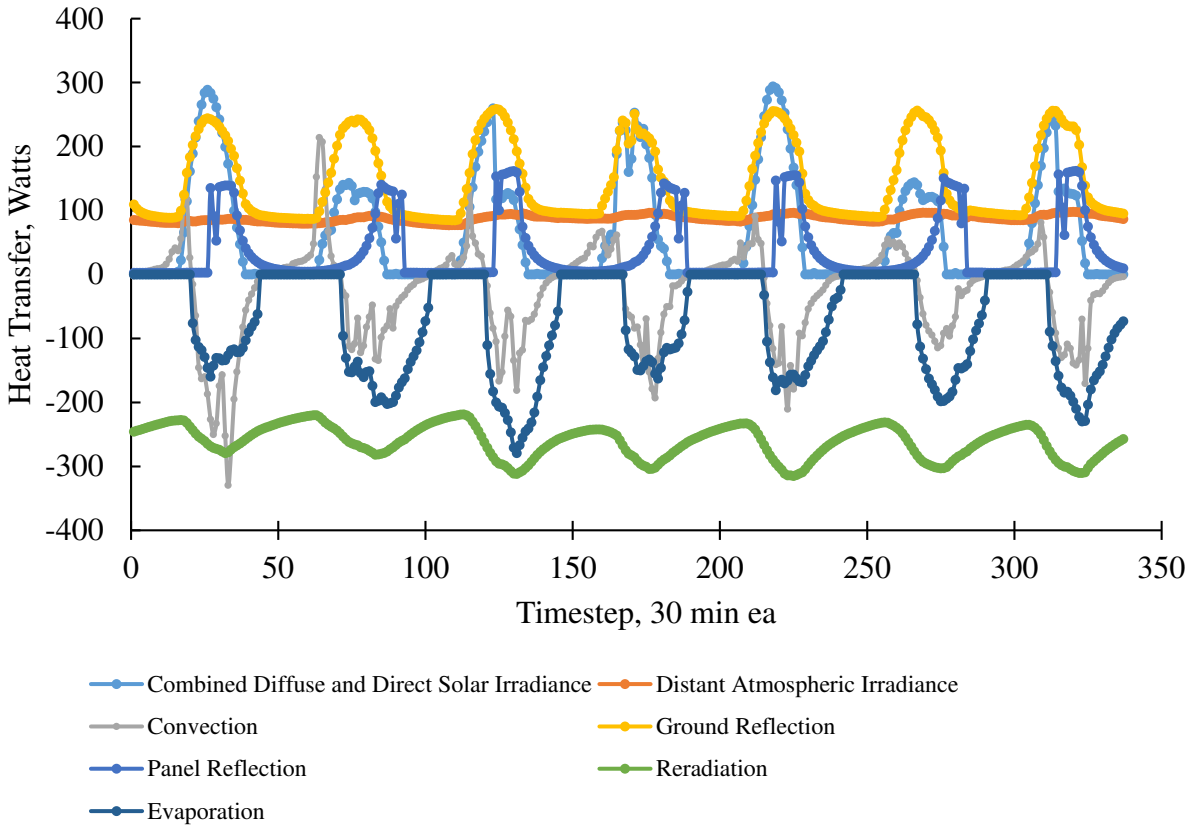

Figure 4: Plot of the relative rates of heat transfer for a model calculation of a week beginning 9/22 in Scottsdale, Az. Values shown are for an interior panel among an array of 5 panels

Open Raceway Pond Heat Fluxes

Direct and diffuse irradiance of ORP

Since the surface of the ORP receiving direct and diffuse irradiance is generally horizontal with respect to the earth's surface, composite values of global horizontal irradiance are utilized to summarize the contributions of both direct and diffuse solar irradiance. Accordingly, the heat transfer due to direct irradiance of the ORP surface is calculated as follows [7,11]

$$Q_{solar} = GHI \cdot \alpha \cdot \tau \cdot A_s \qquad [58]$$

Where A_s is the pond surface area.

Atmospheric distant irradiance of ORP

The distant, longwave, irradiance of an ORP is calculated as:[7,7]:

$$Q_{atmo} = T_{sky}^4 \cdot \alpha \cdot \tau \cdot A_s \quad [59]$$

Conduction to ground

The methodology for predicting heat transfer via conduction to the ground through the bottom of an ORP is adapted from Bechet et al.[11]:

$$L_{ref} = 4400 \cdot ב^{\frac{1}{2}} \qquad [60]$$

$$Q_{ground} = k \cdot \frac{\left(T - T_{ground_{ref}}\right)}{L_{ref}} \cdot A_s \qquad [61]$$

Where L_{ref} is the conduction reference length in meters [11], ב is the thermal diffusivity of the ground, and k is the thermal conductivity of the ground.

Reradiation from the ORP

Similar to the VFP, radiation emanating from the ORP is calculated by [3,4,7,11],

$$Q_{reradiation} = \sigma \cdot \varepsilon \cdot T^4 \cdot A_s \qquad [62]$$

Convection at the ORP surface

Since the brim of the ORP's examined in this study extends slightly above the culture surface, the air velocity across the surface of the culture within the ORP is assumed to be zero. Therefore, only natural convection is considered, calculated as:

$$Q_{convec} = A_s \cdot h \cdot (T_{amb} - T) \qquad [63]$$

The same correlations to determine h in S3.9 are used for the ORP surface.

Evaporation of water from the ORP surface

Evaporation from the surface of the ORP is calculated in the same manner as the method presented in S3.9.

Numerical Integration Schemes

Two numerical time-integration schemes are used in this study. Growth and culture conditions are integrated numerically in time via an explicit, first-order, Euler scheme [8]

$$U_{n+1} = U_n + U'_n \cdot dt \quad [64]$$

Where U is the variable of interest which, in the majority of its implementation in this study, is algal biomass concentration. Alternatively, temperatures are integrated in time via a 4th order Runge-Kutta scheme [8] summarized below:

$$T1_{n+\frac{1}{2}} = T_n + \frac{1}{2} dt \cdot T'_n \qquad [65a]$$

$$T2_{n+\frac{1}{2}} = T_n + \frac{1}{2} dt \cdot T1'_{n+\frac{1}{2}} \qquad [65b]$$

$$T3_{n+1} = T_n + dt \cdot T2'_{n+\frac{1}{2}} \qquad [65c]$$

$$T_{n+1} = T_n + \frac{1}{6}dt \cdot \left[T'_n + 2 \cdot \left(T1'_{n+\frac{1}{2}} + T2'_{n+\frac{1}{2}}\right) + T3'_{n+1}\right] \quad [65]$$

In each case, the dt term is the time step size in seconds. This scheme is applied to the following differential equation, solved for the $\frac{dT}{dt}$ term:

$$\rho C_p V \frac{dT}{dt} = \sum Q_n \qquad [66]$$

With each component of the summation, $\sum Q_n$, calculated at and with each intermediate temperature in the system of equations, T1-T summarized in equation [65]. Noteworthy is that the isolated $\frac{dT}{dt}$ term depends primarily on Q_n, therefore calculation of the derivative terms T1'-T' depends on performing the transient energy balance summarized in equation 66 with the respective temperature for that point in the sequence of [65a] through [65].

Cast Study Inputs

VFP Case Study inputs

Table 3 below summarizes the VFP operating variable inputs for each of the three case studies presented in the manuscript. Refer to Table 7 for applicable strain characteristic inputs.

Table 3: Input parameters for VFP case studies

Parameter	**Value**	**Unit**
Initial Concentration	100	g m^{-3}
Harvest Concentration	300	g m^{-3}
VFP Width	1.156	m
VFP Height	1	m
VFP Depth	0.0381	m

Number of Panels	4	Dimless
Compass Orientation	90	CCW deg
Time Step Size	30	min
Start Date	July 1st	date
Trial Length	168	hours
Culture Density	1000	kg m^{-3}
Strain	*Galdieria sulphuraria*	--
Sparge Gas Addition Rate	15	Liters per minute

ORP Case Study Inputs

Summarized below in Table 4 are the input variables used for each of the three ORP case studies. Refer to Table 1 in the manuscript for applicable strain characteristic inputs.

Table 4: ORP case study inputs

Parameter	**Value**	**Unit**
Initial Concentration	100	g m^{-3}
Harvest Concentration	300	g m^{-3}
Pond Depth	25	cm
Number of Ponds	6	--
Pond Width	1.5	m
Pond Length	3.5	m
Area (calculated)	4.676	$m^{2\ ++}$
Time Step Size	60	min
Start Date	July 1st	date

Trial Length	168	hours
Culture Density	1000	kg m^{-3}
Strain	*Nannochloropsis oceanica*	--

++: Pond is not exactly rectangular, rather area is calculated as:

$$A_s = \frac{\pi}{4} \cdot W^2 + W \cdot (L - W) \qquad [67]$$

Validation Geometries

Vertical Flat Panels at AzCATI

Shown below is an image of the vertical flat panel geometry used at AzCATI during validation of the growth and temperature model developed in this study. An accompanying table and reproduction drawing summarize the pertinent operating and geometric characteristics of the system used during validation of the model developed in this study.

Figure 5: Picture of VFP array at AzCATI. The shading panels on the ends are to provide consistent conditions between all panels, eliminating exceptional irradiance for the end panels. Validation comparison was performed with interior panels only.

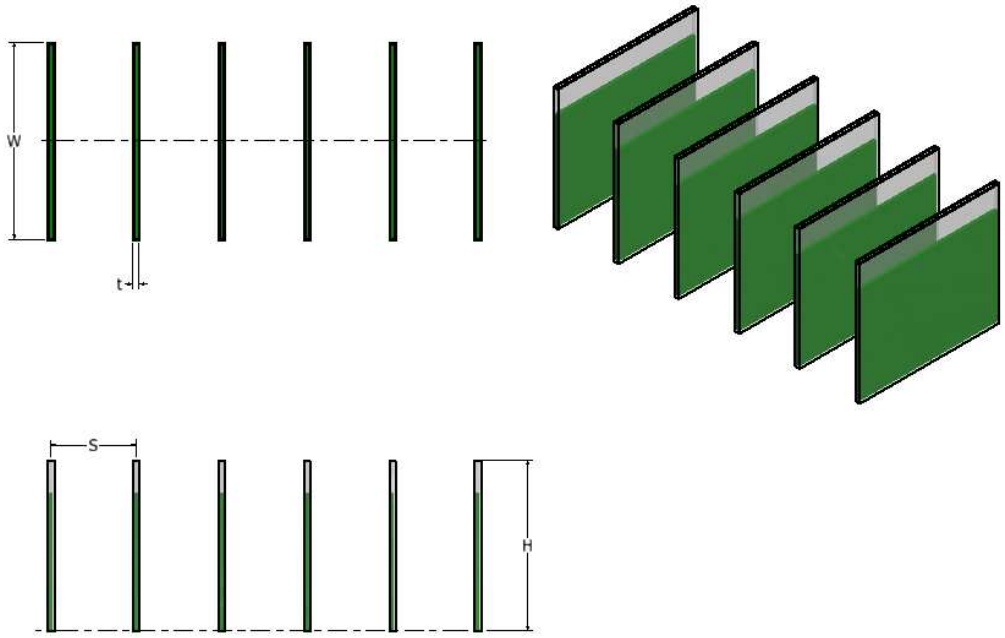

Figure 6: Reproduction drawing illustrating key dimensions of VFP's used in validating the model developed in this study.

Table 5: Summary of pertinent geometric and operating parameters for VFP's used in validating the model developed in this study.

Parameter	**Value**	**Unit**
W	1.156	m
H	1	m
t	0.0381	M
S	0.50	M
Number of Panels	6	Dimless
Compass Orientation	90	CCW deg
Sparge Gas Addition Rate	15	Liters per minute
Sparge Gas % CO2	2	%

Each trial was initialized with media concentrations of the composition shown in Table 6.

Table 6: Growth media for vertical flat panel trials performed at AzCATI

Chemical	Common name	g/L
$(NH_4)_2SO_4$	Ammonium sulfate	1.32
KH_2PO_4	Potassium phosphate Monobasic	0.1
NaCl	Sodium Chloride	0.12
$MgSO_4 \cdot 7H_2O$	Magnesium Sulphate	0.25
$CaCL_2 \cdot 2H_2O$	Calcium Chloride	0.07
$FeCl_3$	Ferric chloride solution (1.45 g/L)	1
	Vitamin solution	0.25
	Sulfuric acid	0.4
NaCl	Sodium Chloride	1
Na_2SO_4	Sodium sulfate	2.8

ORP's Used in ATP3 Testbed Trials

Shown in Figure 7 is an image with dimensions, of the ORP used in the ATP3 trials to which the model in this study was compared. These ORP's were operated at AzCATI and the Georgia Institute of Technology. Each pond was 25 cm deep, 3.5 m long and 1.5 m wide. [12]. PH was maintained by an automated control system with periodic carbon dioxide input to lower PH and sodium hydroxide addition to boost pH to a range between 7.0 and 8.0 for each of the three strains used [12]. Growth media was added at the intervals and composition described by McGowen et al[12] and Harmon et al.[13].

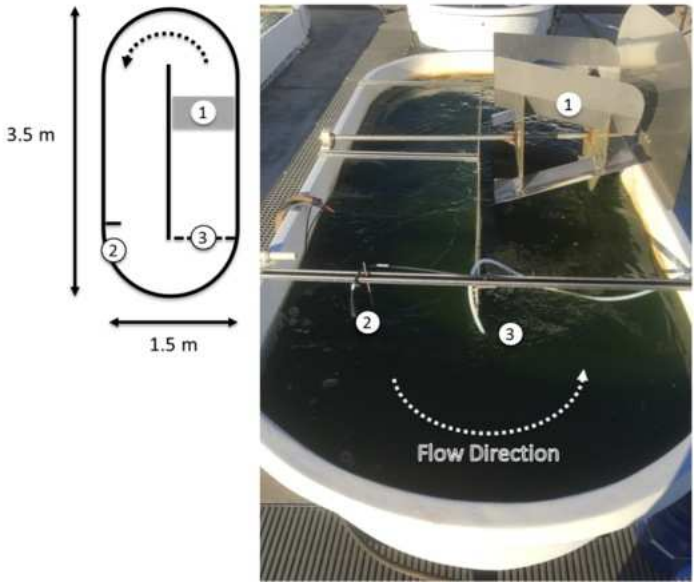

Figure 7: Summary of ATP3 Testbed minipond ORP used for validation comparison of the model developed in this study.

Initial Conditions:

In each of the case studies shown in this study, the initial temperature of the ORP or VFP was set to the ambient air temperature. Though this is likely a somewhat coarse assumption, sensitivity analysis suggests that the model t-ratio response to alterations in ambient temperature are within 0.5. Moreover, any other initial temperature selection represents an equally arbitrary temperature selection. The thermal model developed in this study appears to consistently converge to a periodic steady-state temperature; therefore the initial temperature is considered a nominal and necessarily arbitrary selection. During validation of the thermal model, the pond or VFP temperature was set to the same temperature as the measured experimental temperature at that point in time.

The initial concentration was a user input in the case studies presented in this study. The selection of 100 g m^{-3} is an arbitrary one. Further studies may target this value for optimization, however, doing so was beyond the scope of this study. Likewise, the 300 g m^{-3} harvest

concentration was an equally arbitrary selection, though this selection appears casually consistent with experimental trials. Similar to initial temperature settings during validation, each of the validation trial comparisons was initialized with the measured concentration of the experimental VFP or ORP.

Harvests are simulated in each of the case studies by determining the net difference in biomass between inoculation and the present harvest, storing that value, and resetting the growth unit concentration to the inoculation value. The ORP case studies were set to harvest when concentration reached either 300 g m^{-3} or 5 days had elapsed since the last harvest, whichever came first. VFP harvests were set to occur when concentration reached 300 g m^{-3}.

Approximation of spectral absorptivity and Joule to mol Photon conversion factor

The value of α, absorptivity, used in this study to describe an algal culture is calculated based on the following method provided by Bergman et al.[7]:

$$\alpha = \int_0^\infty \frac{(\alpha_\lambda(\lambda) \cdot E_{\lambda,b}(\lambda,5800K)d\lambda)}{\int_0^\infty (E_{\lambda,b}(\lambda,5800K)d\lambda)} \qquad [68]$$

$$\alpha_\lambda(\lambda) = 1 \text{ for } 400\ nm \leq \lambda \leq 700\ nm \qquad [69]$$

$$\alpha_\lambda(\lambda) = 0 \text{ for } \lambda < 400\ nm\ \&\ \lambda > 700\ nm \quad [70]$$

$$\alpha = 0.356 \qquad [71]$$

Where $E_{\lambda,b}(\lambda, T)$ is the emission from a blackbody at temperature T, assumed in this case to be 5800 K for daylight, and λ wavelength in nanometers. The assumption underlying the equations above is that an algal culture is perfectly absorptive in the photosynthetically active spectrum ($\approx 400\ to\ 700\ nm$) and otherwise perfectly reflective or transparent. Since the meteorological data

used in this study reports solar irradiance in W m^{-2} or J m^{-2} s^{-1}, a method for correlating Joules to photons for sunlight must be established. Therefore the following approach is utilized [5,7]

$$\eta = \frac{\int_{\lambda 1}^{\lambda 2}\left(B(\lambda,T)\cdot\frac{\lambda}{h_p c N_a}\cdot d\lambda\right)}{\int_{\lambda 1}^{\lambda 2}(B(\lambda,T)d\lambda)} \qquad [72]$$

$$\eta = 4.56\cdot 10^{-6}\cdot\frac{mol}{J} \qquad [73]$$

Where B is the spectral radiance of a body at wavelength λ and temperature $T = 5800\ K$, h_p is the Planck constant, c is the speed of light, N_a is Avogadro's Number.

Plot of temperature efficiency v. temperature

A plot of temperature efficiency v temperature is shown in Figure 8

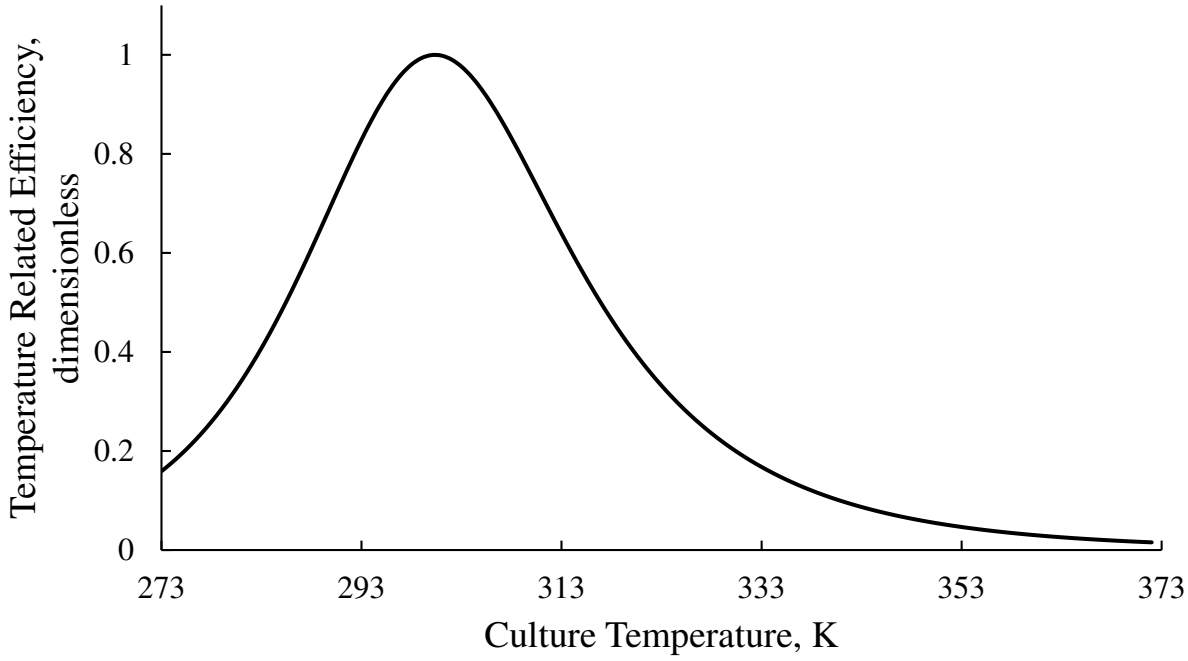

Figure 8: Plot of temperature efficiency v temperature with an optimal temperature at 27.5 C

Full t-ratio plots

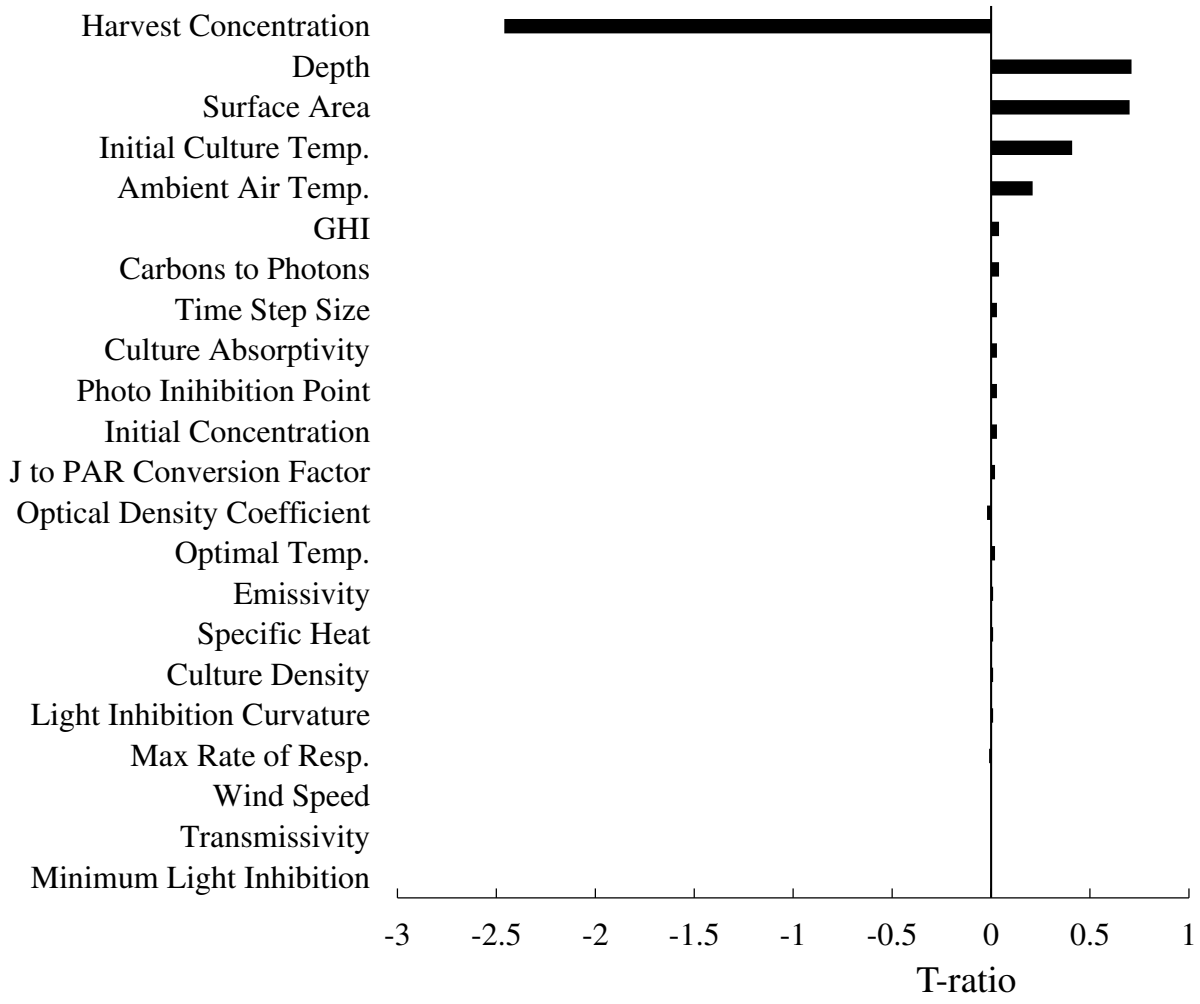

Figure 9: T-ratios for inputs to the coupled thermal-growth model for ORPs. The base case was computed over the first week of July, in Baton Rouge, LA.. Model inputs were altered by ±10% with mass productivity values recorded to evaluate sensitivity.

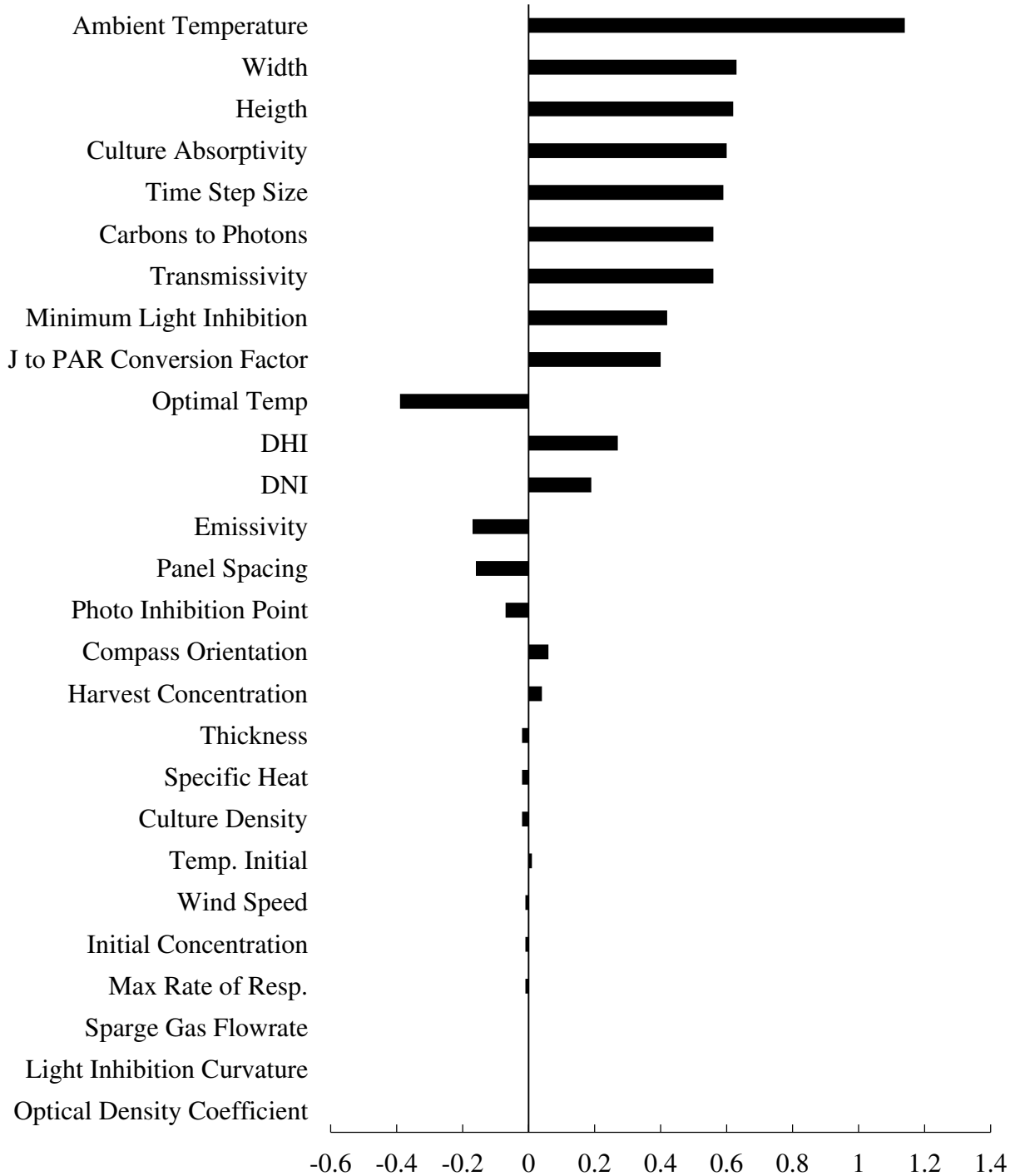

Figure 10: T-ratios for inputs to the coupled thermal-growth model for VFP PBRs. The base case was computed over the first week of July, in Baton Rouge, LA.. Model inputs were altered by ±10% with mass productivity values recorded to evaluate sensitivity.

Plot of Concentration v time in a VFP PBR array

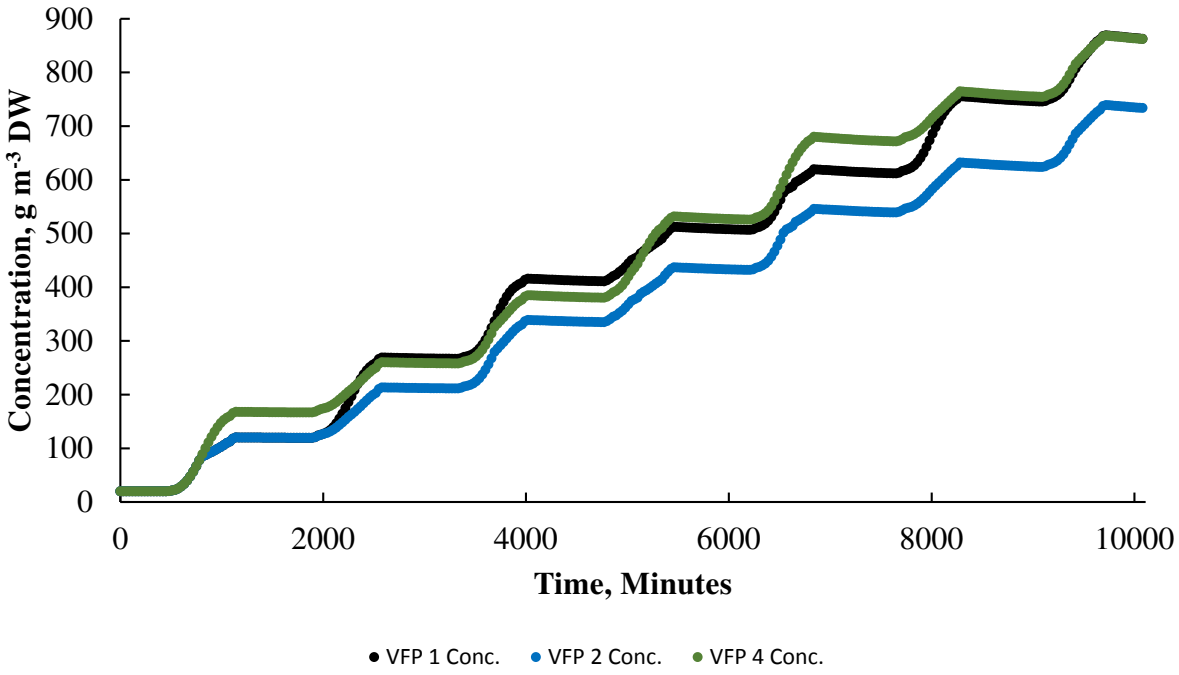

Figure 11: Plot of concentration of dry weight, in grams per meter cubed, over time. Values were generated from a model of 4 units within an array of VFP PBR's operated in September in Scottsdale, Az. VFP 1 and VFP 4 are the end units with VFP 2 being one of the two interior units. Each unit was initialized with a concentration of 20 g m^{-3}.

Error Formulas

$$\%_{error} = \frac{|Y_{exp} - Y_{model}|}{Y_{exp}} \qquad [10]$$

$$Err = |Y_{exp} - Y_{model}| \qquad [11]$$

Where Y is either the algal biomass concentration in g m^{-3} or temperature in K. To exclude experimental growth results that are not representative of typical growth system performance for the VFP PBR, experimental trial results that showed a ratio of final biomass per total irradiance for the trial period more than one standard deviation from the average were not considered in the validation process.

Thermal model accuracy plots

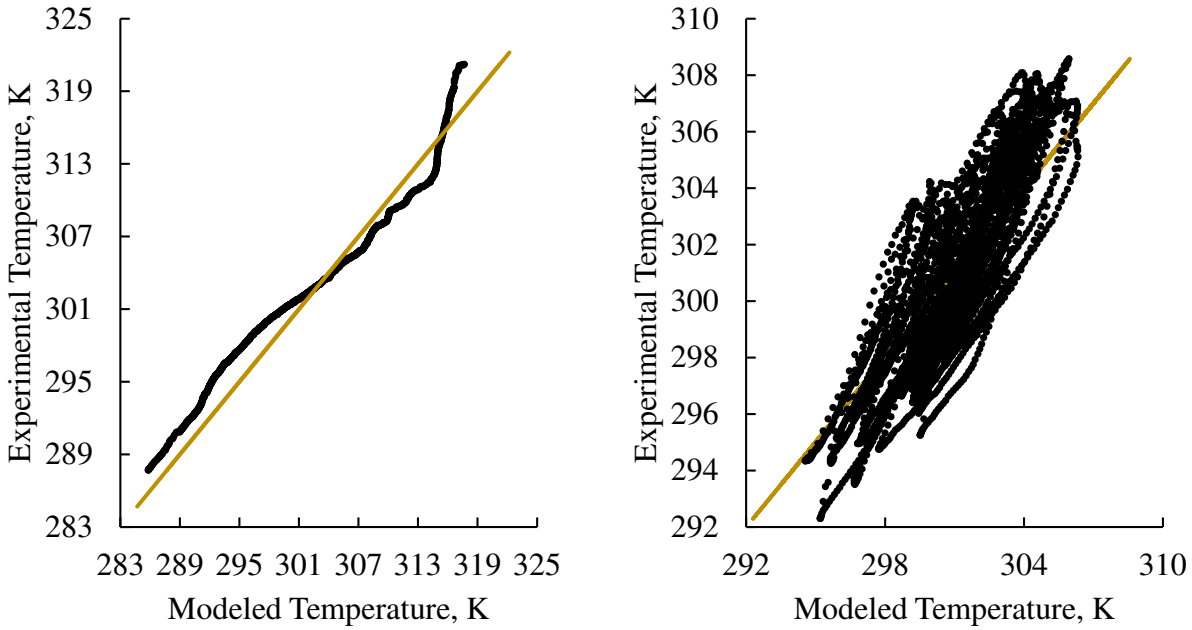

Figure 12: A) A comparison between modeled and experimental temperatures for a VFP PBR. B) A comparison of modeled and experimental temperatures for an ORP1

Table of variables, values, and sources

Table 7: Table of variables, constants, and their sources

Symbol	Variable	Value	Unit	Source
Cx	Biomass Concentration	Varies	g m^{-3}	---
φ_L	Light inhibition efficiency	Varies	Dimless	---
φ_T	Temperature efficiency	Varies	Dimless	---
φ_C	Concentration efficiency	Varies	Dimless	---
P	Incident Light for Photosynthesis	Varies	W	---
D	Decay Rate	Varies	g s^{-1}	---
V	Volume	Varies	m^3	---

$\emptyset_{photon}$	Photon to carbon conversion factor	12/18	mol C / mol Photon	[1,14]
β	Respiration rate	Varies	$\mu g_{biomass}$ g^{-1} s^{-1}	---
$\emptyset_{respiration}$	Respiration rate	Varies	g s^{-1}	---
Q_{direct}	Direct irradiance	Varies	W	---
DNI	Direct Normal Irradiance	Varies	W m^{-2}	[15]
α	Spectral Absorptivity	0.356	Dimless	[7]
τ	Spectral Transmissivity for polyethylene plastic	0.9	Dimless	[7]
A'	Area unshaded of VFP	Varies	m^2	[3,4,16]
δ	Angle between VFP and Sun	Varies	Radians	[3,4,16]
η	Conversion factor between Joules sunlight radiation and PAR Photons	4.56e-6	mol J^{-1}	[5,7]
I_n	Incident radiation contributing to photosynthesis	Varies	W	---
$F(T)$	Intermediate variable in calculating φ_T	Varies	Dimless	[17]
Ea	Activation energy for photosynthesis	63	kJ mol^{-1}	[1,17]
R	Gas constant	8.3145	J K^{-1} mol^{-1}	[7]
a	Light inhibition curvature	Varies	Dimless	---
ρ	Culture Density	1000	kg m^{-3}	[7]
C_p	Specific Heat	4180	J kg^{-1} K	[7]

T	Temperature	Varies	K	---
Q_n	Heat	Varies	W	---
Y_{exp}	Experimental Value	Varies	K, g m^{-3}	---
Y_{model}	Model Value	Varies	K, g m^{-3}	---
Err	Error	Varies	K, g m^{-3}	---
$\%_{error}$	Percent Error	Varies	%	---
OD	Optical Density	Varies	Dimless	---
W	Width	Varies	m	---
H	Height	Varies	m	---
W'	Unshaded width	Varies	m	[3,4,16]
H'	Unshaded height	Varies	M	[3,4,16]
$Q_{diffuse}$	Diffuse heat addition	Varies	W	---
DHI	Diffuse Horizontal Irradiance	Varies	W	[15]
F1	View factor for two rectangular areas, perpendicular at a corner	Varies	Dimless	[5]
F2	View factor for two opposed rectangles	Varies	Dimless	[5]
Q_{atmo}	Atmospheric longwave radiation heat transfer	Varies	W	[3,4]
ε_{sky}	Sky Emissivity	0.8	Dimless	[6]
T_{sky}	Distant Sky Temperature	Varies	Dimless	---
Q''_{ground}	Ground heat flux	Varies	W m^{-2}	[3,4,6]

ε_{grnd}	Ground emissivity	0.90	W m^{-2}	[7]
T_{grnd}	Ground Temp	Varies	K	---
A_g	Ground Area	Varies	m^2	---
h	Heat transfer coefficient	Varies	W m^{-2} K^{-1}	---
σ	Stefan-Boltsmann Constant	5.67e-8	W m^{-2} K^{-4}	[7]
Nu	Nusseldt Number	Varies	Dimless	[7]
Ra	Rayleigh Number	Varies	Dimless	[7]
$Q_{ground_{reflected}}$	Radiant heat reflected by the ground	Varies	W	[3,4,6]
ϑ	Reflectivity	Varies	Dimless	[7]
$Q_{interpanel}$	Interpanel Reflection	Varies	W	[4,16]
$Q_{reradiation}$	Panel reradiation	Varies	W	[1,4,16]
T_{amb}	Ambient Temperature	Varies	K	---
c_h	Wind height correction factor	Varies	Dimless	[9]
V'	Adjusted wind velocity	Varies	m s^{-1}	[9]
ReL	Reynolds number	Varies	Dimless	[7]
Pr	Prandtl Number	Varies	Dimless	[7]
K	Thermal conductivity	Varies	W m^{-1} K^{-1}	[7]
NuM	Nusseldt Number for a Mass Transfer Convection Correlation	Varies	Dimless	[7,10]
Sh	Sherwood Number	Varies	Dimless	[7,10]
Sc	Schmidt Number	0.66	Dimless	[7,10]

M''	Mass flux	Varies	kg m^{-2}	---
h_m	Mass transfer convection coefficient	Varies	kg m^{-2}	---
ω_w	Mass fraction water in water	Varies	%	---
ω_{air}	Mass fraction water in air	Varies	%	---
$Q_{convec}II$	Cooling effect due to water evaporation	Varies	W	[10]
Q_{bubble}	Cooling effect due to water evaporation into sparge gas	Varies	W	[7]
Q_{solar}	Heat transfer due to direct irradiance of an ORP	Varies	W	---
GHI	Global horizontal irradiance	Varies	W m^{-2}	[15]
A_s	ORP Surface Area	Varies	m^{-2}	---
ב	Thermal diffusivity of the ground	691.70	m^2 s^{-1}	[7]
L_{ref}	Reference conduction length	Varies	m	[6]
S	Panel Spacing	Varies	m	----
t	Panel thickness	Varies	m	---
λ	Wavelength	Varies	nm	---
$B(\lambda, T)$	Planck distribution	Varies	W sr^{-1} m^{-2} Hz^{-1}	---
N_a	Avogadro's Number	$6.023*10^{23}$	Mol^{-1}	---

Table of biological growth model inputs

Parameter	Value	Unit	Strain	Geometry	Source
Optimal Temp.	28	Celsius	*N. oceanica*	ORP	[18]
Respiration Rate	1017	(µg biomass) g^{-1} s^{-1}	*N. oceanica*	ORP	Empirical from ATP[3]
Optimal Photo-incidence	1030	µE m^{-2} s^{-1}	*N. oceanica*	ORP	[18]
Light Inhibition Curvature	570	-	*N. oceanica*	ORP	Assumed similar to *C. vulgaris*
Optical Density Coefficient	0.597	-	*N. oceanica*	ORP	ATP[3] data
Optimal Temp.	27.5	Celsius	*C. vulgaris*	ORP	[19]
Respiration Rate	186	(µg biomass) g^{-1} s^{-1}	*C. vulgaris*	ORP	Empirical from ATP[3]
Optimal Photo-incidence	600	µE m^{-2} s^{-1}	*C. vulgaris*	ORP	[19]
Light Inhibition Curvature	570	-	*C. vulgaris*	ORP	[19]
Optical Density Coefficient	0.28	-	*C. vulgaris*	ORP	ATP[3] data
Optimal Temp.	27	Celsisus	*D. intermedius*	ORP	[20]
Respiration Rate	868	(µg biomass) g^{-1} s^{-1}	*D. intermedius*	ORP	Empirical from ATP[3]
Optimal Photo-incidence	500	µE m^{-2} s^{-1}	*D. intermedius*	ORP	[20]
Light Inhibition Curvature	570.3	-	*D. intermedius*	ORP	Assumed similar to *C. vulgaris*
Optical Density Coefficient	0.715	-	*D. intermedius*	ORP	ATP[3] Data

Optimal Temperature	43	Celsius	*G. sulphuraria 5587.1*	ORP	Lammers, unpublished observation
Respiration Rate	136	(µg biomass) g^{-1} s^{-1}	*G. sulphuraria 5587.1*	ORP	Empirical from AzCATI Data
Optimal Photo-incidence	230	µE m^{-2} s^{-1}	*G. sulphuraria 5587.1*	ORP	[21]
Light Inhibition Curvature	57370	-	*G. sulphuraria 5587.1*	ORP	[21]
Optical Density Coefficient	0.406	-	*G. sulphuraria 5587.1*	ORP	AzCATI
Optimal Temperature	35.0	Celsius	*G. sulphuraria Soos*	ORP	[22]
Respiration Rate	124	(µg biomass) g^{-1} s^{-1}	*G. sulphuraria Soos*	ORP	Empirical from AzCATI Data
Optimal Photo-incidence	500	µE m^{-2} s^{-1}	*G. sulphuraria Soos*	ORP	Empirical adjustment
Light Inhibition Curvature	57370	-	*G. sulphuraria Soos*	ORP	[21]
Optical Density Coefficient	0.480	-	*G. sulphuraria Soos*	ORP	AzCATI

Table 8: Table of biological growth model inputs

APPENDIX REFERENCES

(1) Quinn, J.; de Winter, L.; Bradley, T. Microalgae bulk growth model with application to industrial scale systems. *Bioresour. Technol.* **2011**, *102* (8), 5083–5092.

(2) Gim, G. H.; Ryu, J.; Kim, M. J.; Kim, P. I.; Kim, S. W. Effects of carbon source and light intensity on the growth and total lipid production of three microalgae under different culture conditions. *J. Ind. Microbiol. Biotechnol.* **2016**, *43* (5), 605–616.

(3) Slegers, P. M.; Wijffels, R. H.; van Straten, G.; van Boxtel, A. J. B. Design scenarios for flat panel photobioreactors. *Appl. Energy* **2011**, *88* (10), 3342–3353.

(4) Endres, C. H.; Roth, A.; Brück, T. B. Thermal Reactor Model for Large-Scale Algae Cultivation in Vertical Flat Panel Photobioreactors. *Environ. Sci. Technol.* **2016**, *50* (7), 3920–3927.

(5) Howell, J. R.; Menguc, M. P.; Siegel, R. *Thermal Radiation Heat Transfer*, 5th ed.; CRC Press, 2010.

(6) Béchet, Q.; Shilton, A.; Fringer, O. B.; Muñoz, R.; Guieysse, B. Mechanistic Modeling of Broth Temperature in Outdoor Photobioreactors. *Environ. Sci. Technol.* **2010**, *44* (6), 2197–2203.

(7) Bergman, T. L.; Lavine, A. S.; Incropera, F. P.; Dewitt, D. P. *Fundamentals of Heat and Mass Transfer*, 7th ed.; John Wiley & Sons, Inc., 2011.

(8) Lomax, H.; Pulliam, T. H.; Zingg, D. W. *Fundamentals of Computational Fluid Dynamics*, 2nd ed.; Scientific Computation; Springer-Verlag: Berlin, 2003.

(9) Justus, C. G.; Mikhail, A. Height Variation of Wind Speed and Wind Distributions Statistics. *Geophys. Res. Lett.* **1976**, *3* (5), 261–264.

(10) Murphy, T. E.; Berberoglu, H. Temperature fluctuation and evaporative loss rate in an algae biofilm photobioreactor. *J. Sol. Energy Eng.* **2012**, *134* (1), 011002.

(11) Béchet, Q.; Shilton, A.; Park, J. B. K.; Craggs, R. J.; Guieysse, B. Universal Temperature Model for Shallow Algal Ponds Provides Improved Accuracy. *Environ. Sci. Technol.* **2011**, *45* (8), 3702–3709.

(12) McGowen, J.; Knoshaug, E. P.; Laurens, L. M. L.; Dempster, T. A.; Pienkos, P. T.; Wolfrum, E.; Harmon, V. L. The Algae Testbed Public-Private Partnership (ATP 3) framework; establishment of a national network of testbed sites to support sustainable algae production. *Algal Res.* **2017**, *25*, 168–177.

(13) Harmon, V. L.; Dempster, T. A.; McGowen, J. A. *ATP3 Unified Field Study Data*; ATP3 Unified Field Study Data; Dataset; US Department of Energy: Arizona (ASU), California (CP), Florida (FA), Georgia (GT), and Hawaii (CELL).

(14) Wilhelm, C.; Jakob, T. From photons to biomass and biofuels: evaluation of different strategies for the improvement of algal biotechnology based on comparative energy balances. *Appl. Microbiol. Biotechnol.* **2011**, *92* (5), 909–919.

(15) Wilcox, S.; Marion, W. *Users manual for TMY3 data sets*; National Renewable Energy Laboratory Golden, CO, 2008.

(16) Quinn, J. C.; Turner, C. W.; Bradley, T. H. Scale-Up of flat plate photobioreactors considering diffuse and direct light characteristics. *Biotechnol. Bioeng.* **2012**, *109* (2), 363–370.

(17) Alexandrov, G. A.; Yamagata, Y. A peaked function for modeling temperature dependence of plant productivity. *Ecol. Model.* **2007**, *200* (1–2), 189–192.
(18) Sandnes, J. M.; Källqvist, T.; Wenner, D.; Gislerød, H. R. Combined influence of light and temperature on growth rates of Nannochloropsis oceanica: linking cellular responses to large-scale biomass production. *J. Appl. Phycol.* **2005**, *17* (6), 515–525.
(19) Wilson, K. E.; Huner, N. P. The role of growth rate, redox-state of the plastoquinone pool and the trans-thylakoid ΔpH in photoacclimation of Chlorella vulgaris to growth irradiance and temperature. *Planta* **2000**, *212* (1), 93–102.
(20) Vanags, J.; Kunga, L.; Dubencovs, K.; Galvanauskas, V.; Grīgs, O. Influence of Light Intensity and Temperature on Cultivation of Microalgae Desmodesmus Communis in Flasks and Laboratory-Scale Stirred Tank Photobioreactor. *Latv. J. Phys. Tech. Sci.* **2015**, *52* (2), 59–70.
(21) Oesterhelt, C.; Schmälzlin, E.; Schmitt, J. M.; Lokstein, H. Regulation of photosynthesis in the unicellular acidophilic red alga Galdieria sulphuraria†: Regulation of photosynthesis in Galdieria. *Plant J.* **2007**, *51* (3), 500–511.
(22) Gross, W.; Oesterhelt, C.; Tischendorf, G.; Lederer, F. Characterization of a non-thermophilic strain of the red algal genus *Galdieria* isolated from Soos (Czech Republic). *Eur. J. Phycol.* **2002**, *37* (3), 477–482.